Mahoney, J.J., Fitton, J.G., Wallace, P.J., et al., 2001
Proceedings of the Ocean Drilling Program, Initial Reports Volume 192

2. Explanatory Notes[1]

Shipboard Scientific Party[2]

INTRODUCTION

Introduction

Information in this chapter concerns only the shipboard operations and analyses used for producing the site chapters of the Leg 192 *Initial Reports* volume of the *Proceedings of the Ocean Drilling Program*. Methods used by various investigators for shore-based analyses of Leg 192 data will be described in the individual scientific contributions to be published in the *Scientific Results* volume and elsewhere.

Authorship

The Leg Summary (Chapter 1) and separate sections of the site chapters were written by the following shipboard scientists (authors are listed below in alphabetical order; no seniority is implied).

Leg Summary: Godfrey Fitton, John Mahoney
Background and Objectives: Mike Coffin, Godfrey Fitton, John Mahoney
Operations: Ron Grout, Paul Wallace
Lithostratigraphy: Ken MacLeod, Hajime Naruse, Jim Ogg, Wietze van der Werff
Biostratigraphy: Jim Bergen, Paul Sikora
Igneous Petrology: Pat Castillo, Lynne Chambers, Bill Chazey, Marguerite Godard, Stephanie Ingle, Clive Neal, Takashi Sano, Paul Wallace, Rosalind White
Alteration: Neil Bannerjee, José Honnorez
Structural Geology: Wietze van der Werff
Paleomagnetism: Stuart Hall, Peter Riisager
Physical Properties: Maria Antretter, Loren Kroenke, Xixi Zhao

[1]Examples of how to reference the whole or part of this volume.
[2]Shipboard Scientific Party addresses.

Ms 192IR-102

Downhole Measurements: Graeme Cairns, Mike Coffin
Core Descriptions: Shipboard Scientific Party

"Core Descriptions" includes summary core descriptions (barrel sheets), core photographs, and thin section descriptions.

Shipboard Scientific Procedures

Numbering of Sites, Holes, Cores, and Samples

Ocean Drilling Program (ODP) drill sites are numbered consecutively. Each site consists of one or more holes drilled while the ship was positioned over one acoustic beacon. For all ODP drill sites, a letter suffix distinguishes individual holes drilled at the same site. We assign the first hole drilled the site number modified by the suffix A; the second hole takes the site number and suffix B, and so forth. This procedure, which differs slightly from that used by the Deep Sea Drilling Project (DSDP) (Sites 1–624), prevents ambiguity between site- and hole-number designations. Distinguishing among holes drilled at a site is important because sediments or rocks recovered from different holes usually do not come from exactly equivalent positions in the stratigraphic column.

We measure the cored interval in meters below the seafloor (mbsf). The depth interval assigned to an individual core begins with the depth below the seafloor at which coring began and extends to the depth that coring ended. Each coring interval is generally ≤9.5 m, which is the length of a core barrel. Coring intervals may be shorter and may not necessarily be adjoining if separated by drilled intervals that are not cored. In soft sediments, the drill string can be "washed ahead" with the core barrel in place, without recovering sediments. This is achieved by pumping water down the pipe at high pressure to wash the sediment out of the way of the bit and up the space between the drill pipe and the wall of the hole. In drilling hard rock, a center bit may replace the core barrel if it is necessary to drill without coring.

Cores taken from a hole are numbered sequentially from the top of the hole downward. Core numbers and their associated cored intervals in meters below the seafloor are unique in a given hole. Normally, maximum recovery for a single core is 9.5 m of rock or sediment contained in a plastic liner (6.6 cm internal diameter) plus ~0.2 m (without a plastic liner) in the core catcher (Fig. **F1**). The core catcher is a device at the bottom of the core barrel that prevents the core from sliding out when the barrel is being retrieved from the hole. In certain situations recovery may exceed the 9.5-m maximum. In hard-rock cores, this probably happens when a pedestal of rock fails to break off and be grabbed by the core catcher. When a subsequent core barrel is deployed, this pedestal enters the core barrel and, because it is from the previous cored interval, it can lead to >9.5 m of recovery from the next 9.5-m cored interval.

A recovered core is divided into 1.5-m sections that are numbered serially from the top (Fig. **F1**). When full recovery is obtained, the sections are numbered from 1 through 7, with the last section usually being shorter than 1.5 m (rarely, an unusually long core may require more than seven sections). When less than full recovery is obtained, as many sections as are needed to accommodate the length of the core are used; for example, 4 m of core would be divided sequentially into two 1.5-m sections (1 and 2) and a 1-m section (3). If cores are fragmented and recovery is <100%, sections are numbered sequentially and the rest of the

F1. Schematic examples of core sections, p. 37.

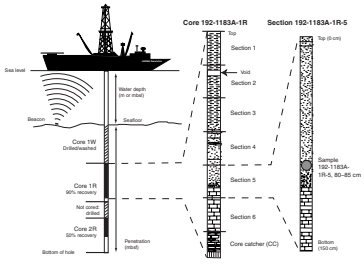

cored interval is regarded as void, whether or not shipboard scientists think that the fragments were contiguous when in situ. In rare cases, a section <1.5 m long may be cut to preserve features of interest (e.g., lithologic contacts).

By convention, material recovered from the core catcher is placed below the last section when the core is described and is labeled "core catcher" (CC); in sedimentary cores, it is treated as a separate section. The core catcher is placed at the top of the cored interval in cases in which material is recovered only in the core catcher. However, information supplied by the drillers or by logging may allow more precise interpretation as to the correct position of core catcher material within an incompletely recovered cored interval.

By convention, when the recovered core is shorter than the cored interval, the top of the core is equated with the top of the cored interval. Samples taken from the cores are designated by distance measured in centimeters from the top of the section to the top and bottom of each sample.

A complete identification number for a sample consists of the following information: leg, site, hole, core number, core type, section number, piece number (assigned only for igneous rock and sedimentary rock interbedded with igneous rock), and interval in centimeters measured from the top of the section. For example, as in Figure **F1,** a sample identification of "192-1183A-1R-5, 80–85 cm" indicates a 5-cm sample removed from the interval between 80 and 85 cm below the top of Section 5 of Core 1 (R indicates that this core was taken during rotary drilling) of Hole 1183A during Leg 192.

Core Handling

Sediments

As soon as a core is retrieved on deck, a sample is removed from the core catcher and taken to the paleontology laboratory for an initial age assessment. Then the core is laid out on a long horizontal rack on the catwalk adjacent to the drilling floor. The core is marked into section lengths, each section is labeled, and the core is cut into sections. Headspace gas samples are taken from the ends of cut sections on the catwalk and sealed in glass vials for light hydrocarbon analysis as part of the shipboard safety and pollution-prevention program. During Leg 192, we only took headspace gas samples of sediment at Site 1185. The plastic core liner containing each section then is sealed at the top and bottom by gluing on color-coded plastic caps: blue to identify the top of a section and clear to identify the bottom. The caps are usually attached to the liner by coating the end of the liner and the inside rim of the cap with acetone.

Next, the sections of core are carried into the laboratory, and each is labeled again using an engraver to mark the full designation of the section permanently onto the plastic core liner. The length of the core in each section and of the core catcher sample is measured to the nearest centimeter; this information is logged into the shipboard CORELOG database program. After cores have equilibrated to room temperature (~3 hr), they are passed through the multisensor track (MST). Thermal conductivity measurements are made on relatively soft sediments and the cores are split.

Cores of soft material are split lengthwise into working and archive halves. Softer cores are split with a wire or saw, depending on the degree

of induration. Harder cores are split with a band saw or diamond saw. During Leg 192, we split the wire-cut cores from the bottom to top; thus, older material may have been transported up the core on the split face of each section.

The working half of the core is next sampled for both shipboard and shore-based laboratory studies. Each sample extracted is logged into the sampling computer's database program and identified by the sample's location and the name of the investigator receiving the sample. The curator at ODP keeps records of all samples removed from the core. Samples are sealed in plastic vials or bags and labeled. Samples for shipboard physical properties (PP) measurements and for calcium carbonate (coulometric) analysis are taken routinely.

The archive half of the core is described visually and smear slides are made from sediment samples taken from this half. Most archive sections are run through the cryogenic magnetometer. The archive half then is photographed using both black-and-white and color film, an entire core at a time. Close-up photographs (color and black-and-white) of particular features are taken as requested by individual scientists for illustrations in the *Initial Reports* volume.

Both halves of the core then are placed into labeled plastic tubes, sealed, and transferred to cold-storage space aboard the drilling vessel. At the end of the leg, the cores are transferred from the ship in refrigerated air-freight containers to cold storage at ODP's Gulf Coast Repository at Texas A&M University.

Igneous and Metamorphic Rocks

Igneous rock cores are handled differently from sedimentary cores. To minimize contamination of cores with platinum-group elements and gold, scientists and technicians removed all jewelry from their hands and wrists before handling the core. Once on deck, the core catcher sample is placed at the bottom of the core liner, and total core recovery is calculated by pushing the rock pieces together and measuring the total length to the nearest centimeter. This information is logged into the shipboard CORELOG database program. Then the core is cut into 1.5-m-long sections and transferred to the laboratory.

The contents of each section are transferred into 1.5-m-long sections of split core liner where the bottoms of oriented pieces (i.e., pieces that clearly could not have rotated top to bottom about a horizontal axis in the liner) are marked with a red wax pencil. This ensures that orientation is not lost during splitting and labeling. Important primary features of the cores are recorded at this time. The core then is split into archive and working halves. A plastic spacer separates individual pieces and/or reconstructed groups of pieces in the core liner. These spacers may represent a substantial interval of no recovery. Each piece is numbered sequentially from the top of each section, beginning with number 1; reconstructed pieces are all assigned the same number but with a consecutive suffix letter (e.g., Piece 1A, 1B, etc.). Pieces are labeled only on the outer cylindrical surfaces of the core. If the piece is oriented, an arrow pointing to the top of the section is added to the label. Because pieces are free to rotate about a vertical axis during drilling, relative azimuthal orientation during Leg 192 was possible only by using paleomagnetic data.

In splitting the core, every effort is made to ensure that important features are represented in both halves. The archive half is described visually. Most archive sections are run through the cryogenic magneto-

meters. The archive halves are then photographed with both black-and-white and color film, one core at a time. Nondestructive physical properties measurements, such as magnetic susceptibility, are also performed on the archive half of the core. The working half is sampled for shipboard physical properties measurements, paleomagnetic studies, inductively coupled plasma–atomic emission spectrometry (ICP-AES), X-ray diffraction (XRD), and thin section studies. The working half of the hard-rock core then is sampled for shore-based laboratory studies. The curator at ODP keeps records of all samples. After samples are taken, both halves of the core are shrink-wrapped in plastic to prevent rock pieces from vibrating out of sequence during transit, placed into labeled plastic tubes, sealed, and transferred to cold-storage space aboard the drilling vessel. As with the other Leg 192 cores, they are housed at ODP's Gulf Coast Repository at Texas A&M University.

SITE GEOPHYSICS

Sites for Leg 192 were selected on the basis of multichannel seismic (MCS), single-channel seismic (SCS), bathymetric, and sonobuoy data collected during several surveys aboard Japanese and United States ships, in addition to satellite-derived gravity data (Fig. F2). The type and quality of seismic site-survey data vary (see Table T1 for a summary of seismic parameters). One survey (*Thomas Washington* 88-11) was undertaken before the availability of full Global Positioning System (GPS) coverage and thus has less reliable navigation data.

F2. Ontong Java Plateau bathymetry, p. 38.

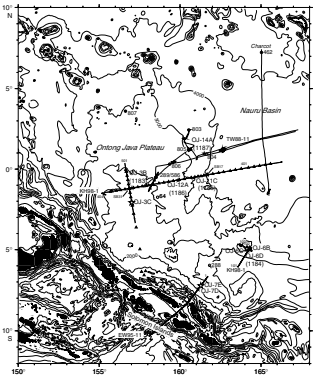

T1. Acquisition parameters of seismic reflection data, p. 45.

Hakuho Maru KH98-1 Leg 2

Japanese, American, and Norwegian scientists aboard the *Hakuho Maru* (KH98-1 Leg 2) acquired ~315 km of 24-channel and ~1795 km of 48-channel seismic reflection data, together with sonobuoy, bathymetric, gravity, and magnetic data, over the Ontong Java Plateau and Nauru Basin in 1998 (Mochizuki et al., 1998; Araki et al., 1998). Portions of the KH98-1 Leg 2 MCS data were used to locate the primary and alternate OJ-3 (central high plateau crest), OJ-6 (eastern salient), OJ-11 (eastern flank of the central plateau), and OJ-12 (eastern slope of the central plateau) sites.

Japan's site survey aboard the *Hakuho Maru* was conducted by the Ocean Research Institute of the University of Tokyo (Principal Investigator/Chief Scientist Asahiko Taira), in collaboration with the Japan Marine Science and Technology Center (JAMSTEC); Chiba University; the Institute for Geophysics, the University of Texas at Austin (MCS data processing); the Department of Geology, University of Oslo, Norway; the Department of Geology and Geophysics, University of Hawaii at Manoa; Graduate School of Oceanography, the University of Rhode Island; and the Department of Earth Sciences, University of North Carolina, Wilmington. Financial support for U.S. scientist involvement was provided by the U.S. National Science Foundation (OCE-9714368; Principal Investigator Millard F. Coffin) and the U.S. Science Support Program (USSSP) of the Joint Oceanographic Institutions (JOI), Inc.

Maurice Ewing 95-11

American and Japanese scientists aboard the *Maurice Ewing* (cruise EW95-11) examined the southwestern flank of the plateau in 1995, col-

lecting ~2000 km of coincident 120-channel seismic reflection, bathymetric, gravity, and magnetic data (Mann et al., 1996; Phinney et al., 1999). The OJ-7 primary and alternate sites (Stewart Arch) are located on an EW95-11 MCS line. However, lack of necessary clearances to drill in the Exclusive Economic Zone of the Solomon Islands prevented drilling of any sites using the EW95-11 MCS data.

The *Maurice Ewing* geophysical program was funded by the U.S. National Science Foundation (OCE-9301608; Principal Investigators/Chief Scientists Paul Mann, Millard F. Coffin, and Thomas H. Shipley), in cooperation with the Ocean Research Institute, University of Tokyo (Principal Investigator/Chief Scientist Kiyoshi Suyehiro), and Chiba University (Principal Investigator Masanao Shinohara).

Thomas Washington 88-11

As part of ODP site surveys for Leg 130 in 1988, scientists aboard the *Thomas Washington* (cruise TW88-11) acquired ~1500 km of digital SCS, bathymetry, gravity, and magnetic data on the Ontong Java Plateau. ODP Sites 803, 804, 805, and 806 were located using the cruise TW88-11 SCS data (Mayer et al., 1991; Mosher et al., 1993). The OJ-14 site (at the foot of the eastern flank of the central plateau) also was located using the TW88-11 SCS data.

Support for the *Thomas Washington* work was provided by the U.S. Office of Naval Research (n00014-91-1213) and the U.S. National Science Foundation (Principal Investigator Edward L. Winterer), in collaboration with the Canadian Secretariat for the Ocean Drilling Program, the Canadian National Scientific and Engineering Research Council, Dalhousie University, and the Département de Géologie Dynamique, Université Pierre et Marie Curie.

LITHOSTRATIGRAPHY

Description of sedimentary deposits recovered during Leg 192 generally followed standard ODP methodology. Thus, most procedures used are only briefly outlined, but, where we depart significantly from ODP conventions, we provide a more detailed explanation. Procedures for the description of igneous rocks are described in "Igneous Petrology," p. 12, "Alteration," p. 17, and "Structural Geology," p. 18.

Visual Core Description

We described each core in detail and entered our observations into AppleCORE (version 8.1f) software. For cores with considerable variation at the meter scale, we first recorded our observations on visual core description (VCD) forms and then condensed and summarized these observations for entry into AppleCORE. AppleCORE generates a simplified, annotated graphical description (barrel sheet) of each core. Barrel sheets are presented alongside corresponding core photographs (see the "Core Descriptions" contents list). AppleCORE also creates a data file of depth-facies information for use in the ODP Janus database.

The lithologies of the sedimentary intervals recovered are represented on barrel sheets by symbols in the column headed "Graphic Lithology" (Fig. F3). Classification follows the scheme of Mazzullo et al. (1988) with minor modifications as outlined below. Bed thickness is characterized as very thick bedded (>100 cm thick), thick bedded (30–

F3. Core description summary (barrel sheet), p. 39.

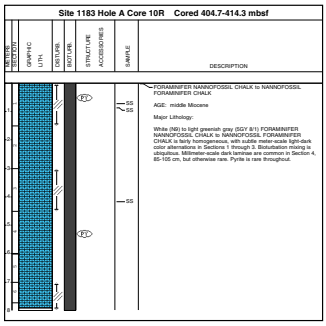

100 cm thick), medium bedded (10–30 cm thick), thin bedded (3–10 cm thick), and very thin bedded (1–3 cm thick) (McKee and Weir, 1953). Grain-size divisions (i.e., sand, silt, clay, etc.) are those of Wentworth (1922). Sediments are represented by a single graphic lithology pattern if they are relatively homogeneous across the interval described. In homogenous sediments with two or three dominant components not described by a single standard lithology pattern, strips are plotted showing the relative abundance of each component.

The stratigraphic distribution of geological features such as degree of bioturbation, primary sedimentary structures, soft-sediment deformation, accessory minerals, discrete trace fossils, and diagenetic features are indicated schematically in columns to the right of the graphic log. Specific stratigraphic information concerning important or unusual discrete structures is listed in the description column. In addition, VCD forms containing the detailed observations can be obtained from ODP. Figure **F4** contains a key to the full set of symbols used on the graphic columns.

Features related to sampling, analysis, and processing of the cores are indicated on the barrel sheets using symbols defined in Figure **F4.** Locations of samples taken for shipboard lithostratigraphic analysis (smear slides, thin sections, carbonate analysis, etc.) are indicated in the "Sample" column, with analysis types represented by the codes listed in Figure **F4.**

The description column summarizes the lithologies observed and the approximate geologic age provided by shipboard paleontological studies. The description generally includes key characteristics of all the major and important minor sediment lithologies (e.g., color, composition, sedimentary structures, and visible trace and body fossils). We estimated general sediment color trends by comparison to Munsell Soil Color Charts (1975). Detailed color data were quantified with an automated color reflectance spectrophotometer (see **"Color Reflectance Spectrophotometry,"** p. 10).

F4. Key to symbols used on barrel sheets, p. 40.

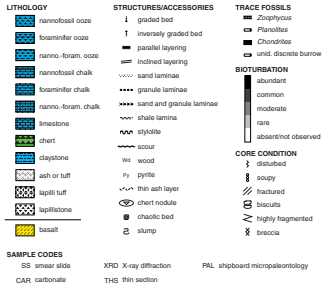

Sediment Classification

Lithologic names consist of a principal name based on composition, degree of lithification, and/or texture. For lithologies with a mixture of components, the principal name is preceded by major modifiers (in order of increasing abundance) that refer to those components making up >25% of the sediment. Names of minor components that represent between 10% and 25% of the sediment follow the principal name after a "with," in order of increasing abundance. Thus, an unconsolidated sediment containing 30% nannofossils, 25% clay minerals, 20% foraminifers, 15% quartz silt, and 10% ferromanganese nodules would be described as a clayey nannofossil ooze with ferromanganese nodules, quartz silt, and foraminifers. These naming conventions follow the ODP sediment classification scheme (Mazzullo et al., 1988), with the exception that during Leg 192 we did not distinguish a separate mixed-sediment category (Fig. **F5**). We did not encounter neritic shallow-water carbonate sediments or chemical sediments except as accessory minerals and do not address these categories below.

Granular sediments are subdivided on the basis of composition and abundance of different grain types estimated from visual examination of the core, smear slides, thin sections, and by shipboard measurements of carbonate content (see **"Inorganic Carbon,"** p. 9) and shipboard XRD analyses (see **"X-Ray Diffraction,"** p. 9). Grain-size divisions are

F5. Granular sediment classification scheme, p. 41.

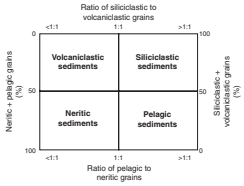

those of Wentworth (1922). For volcaniclastic sediments the term "ash" ("tuff" if lithified) is used in place of sand, and the term "lapilli" is used for granule and cobble size categories. Larger volcanic clasts (breccia) were not encountered. Size-textural qualifiers were not used for pelagic sediment names (e.g., nannofossil clay implies that the dominant component is siliciclastic clay rather than clay-size nannofossils). For thin section analysis of microfacies, we used the textural classification scheme of Dunham (1962). We classified matrix-supported rocks as "mudstone" if they contain <10% and "wackestone" if they contain >10% grains. Grain-supported rocks are classified as "packstone" if clay and silt are present or "grainstone" if silt and clay are absent.

Terms that describe lithification vary depending upon the dominant composition:

1. Sediments derived predominantly from calcareous pelagic organisms (e.g., calcareous nannofossils, foraminifers): the lithification terms ooze, chalk, and limestone reflect whether the sediment can be deformed with a finger (ooze), can be scratched easily by a fingernail (chalk), or cannot be scratched easily (limestone).
2. Sediments derived predominantly from siliceous microfossils (diatoms, radiolarians, and siliceous sponge spicules): the lithification terms ooze, porcellanite, and chert reflect whether the sediment can be deformed with a finger (ooze), cannot be easily deformed manually (porcellanite), or displays a glassy luster (chert). Note that the terms porcellanite and chert do not indicate the mineralogy of the silica.
3. Sediments derived predominantly from siliciclastic material: if the sediment can be deformed easily with a finger, no lithification term is added and the sediment is named for the dominant grain size; for more consolidated material the lithification suffix "-stone" is appended to the dominant size classification (e.g., clay vs. claystone).
4. Sediments composed of sand-size volcaniclastic grains: if the sediment can be deformed easily with a finger, the interval is described as ash; for more consolidated material, the rock is called tuff. The term lapilli is used for clasts that are granule or cobble size, and no distinction is made based on degree of lithification.

Thin Sections and Smear Slides

The sediment names we applied were based largely on analysis of thin sections and smear slides. Tables summarizing data from thin sections and smear slides are included (see the **"Core Descriptions"** contents list). These tables include information about the sample location, whether the sample represents a dominant (D) or a minor (M) lithology in the core, and the estimated abundance of different grain sizes and different grain types. Although we tried to ensure consistency among observers and through time, thin section and smear slide analyses on the ship are qualitative; percentages listed are visual estimates of the relative abundances. The mineral identification of finer grained particles can be difficult using only a petrographic microscope, and the abundance of sand-size grains tends to be underestimated in smear slides because they are often incorporated into the smear unevenly. Classification of limestone facies generally requires a thin section. Additional information on composition was obtained by XRD analysis (see **"X-Ray**

Diffraction," p. 9) and measurement of carbonate content (see "Inorganic Carbon," p. 9).

X-Ray Diffraction

For selected samples, the relative abundances of the main silicate and carbonate minerals were determined with a Philips model PW1729 X-ray diffractometer using Ni-filtered CuK_α radiation. Typical sampling frequency was one per core but was higher in intervals with two or more different lithologies. Each bulk-sediment sample was freeze-dried and crushed. The powder was mounted with a random grain orientation into an aluminum sample holder. Instrument conditions were as follows: 40 kV, 35 mA; goniometer scan from 2° to 70° 2θ for bulk samples; step size of 0.01° 2θ; scan speed at 1.2° 2θ/min; count time of 0.5 s at each step. After converting peak intensities to values appropriate for a fixed slit width, we used an interactive software package (MacDiff 3.3.0 PPC) on a Macintosh computer to identify the main minerals. Most diffractograms were peak-corrected to match the main calcite peak at 3.035 Å. In the absence of both quartz and calcite, no peak correction was applied. Identifications are based on multiple peak matches, using the mineral database provided with MacDiff.

Peak areas were measured only to estimate calcite/dolomite ratios. In all other cases, minerals were grouped as major or trace components, depending on relative peak heights. Accurate estimation of the proportions of clay minerals, glass, or amorphous opal is impossible with the bulk samples used for analysis, although mixtures of these phases with calcite make up most of the analyzed samples. Relative abundances reported in this volume are useful for general characterization of the sediments, but they are not precise, quantitative data.

Inorganic Carbon

Carbonate carbon concentrations were measured using a Coulometrics 5011 CO_2 coulometer. Typical sampling frequency was one per core but was higher in intervals with two or more different lithologies. The coulometer consists of a reaction vessel and a coulometer cell. The coulometer cell is filled with a proprietary solution containing monoethanolamine (ME) and a colorimetric indicator. A platinum cathode and a silver anode are placed in the cell and the cell assembly is positioned between a light source and a photodetector. For samples analyzed during Leg 192, ~10 mg of freeze-dried, ground sediment was acidified with 2-M HCL in the heated reaction vial. The CO_2 evolved is carried on a free air stream through a scrubbing system and into the coulometric cell, where the CO_2 is quantitatively absorbed and reacts with ME to form a titratable acid. Decreased pH causes the colorimetric indicator to fade. The photodetector monitors the change in the solution's color as percent transmittance. An increase in percent transmittance causes a current to be passed through the cell, thereby back-titrating the solution. When the solution returns to its original color, the current stops. The percentage of inorganic carbon (IC) is calculated from the current passed through the cell and the mass of sample analyzed; the weight percentage of carbonate is determined from the IC, with the assumption that all IC is present as calcium carbonate ($CaCO_3$):

$$CaCO_3 \text{ wt\%} = \text{IC wt\%} \times 8.332. \quad (1)$$

Color Reflectance Spectrophotometry

In addition to visual estimates of the color, we routinely measured the reflectance of visible light from cores using a Minolta spectrophotometer (model CM-2002) mounted on the archive multisensor track (AMST). The AMST measures the archive half of each core section and provides a high-resolution stratigraphic record of color variations for visible wavelengths (400–700 nm). We covered freshly split cores with clear plastic wrap and placed them on the AMST, making measurements at a 4- or 5-cm spacing. The AMST skips empty intervals and intervals where the core surface is well below the level of the core liner, but the AMST cannot recognize relatively small cracks or disturbed areas of core. Thus, AMST data may contain spurious measurements that should, to the extent possible, be edited out of the data set before use. Each measurement recorded consists of 31 separate determinations of reflectance in 10-nm-wide spectral bands from 400 to 700 nm. Additional detailed information about measurement and interpretation of spectral data with the Minolta spectrophotometer can be found in Blum (1997), Balsam et al. (1997, 1998), and Balsam and Damuth (2000).

BIOSTRATIGRAPHY

The primary biostratigraphic objective for all Leg 192 sites was to date sediments immediately overlying basement and any intercalated with basalt. Our secondary objective was to estimate sedimentation rates and delineate the location and duration of unconformities and then to compare the results to those obtained from other sites drilled on the Ontong Java Plateau. After we established age estimates, our final objective was to determine paleoenvironments from recovered benthic assemblages and integrate the results with the plateau's history.

We used the timescale and bioevents of Berggren et al. (1995) for Cenozoic strata and the Gradstein et al. (1995) timescale for the Cretaceous. Absolute age estimates for Cretaceous calcareous nannofossil and planktonic foraminifer bioevents are from the database housed at the Energy and Geoscience Institute at the University of Utah. In addition, the recently published "Sequence Chronostratigraphic Chart" of Hardenbol et al. (1998), which was calibrated to the same Mesozoic timescale used during Leg 192 (Gradstein et al., 1995), also provided estimates of absolute age for many Cretaceous microfossil bioevents.

Calcareous Nannofossils

Biostratigraphy

We used the following zonal schemes at all Leg 192 sites: (1) Martini (1971) for the Cenozoic; (2) Sissingh (1977, 1978; CC Zones) for the Campanian–Maastrichtian; (3) Bergen and Sikora (1999) for the Coniacian–Santonian; and (4) Bralower et al. (1993, 1995) for the Aptian–Albian. Bralower et al. (1993) modified the original zonation published by Roth (1978; NC Zones). We also used Perch-Nielsen (1985), Jeremiah (1996), Bown (1998), and Burnett (1997) as references for taxonomy and stratigraphy. A large number of Cretaceous nannofossil events were de-

rived from the data of Bergen (1998), Bergen and Sikora (1999), and J.A. Bergen (unpubl. data) from reference sections in North America, western Europe, and Tunisia.

Methods

We examined calcareous nannofossils by standard light microscope techniques using transmitted light and crossed polarizers at 1000×–1560× magnification. From smear slides, we recorded seven calcareous nannofossil abundance levels as follows:

V = very abundant (100 or more specimens per field of view).
A = abundant (10–99 specimens per field of view).
C = common (1–9 specimens per field of view).
F = few (1 specimen per 2–10 fields of view).
O = occasional (1 specimen per 11–100 fields of view).
R = rare (1 specimen per 101–1000 fields of view).
B = barren.

Planktonic and Benthic Foraminifers

Paleoenvironmental Analysis

Biofacies analyses were performed on the samples recovered, the objectives being to define paleoenvironments and to elucidate depositional conditions through time in conjunction with shipboard sedimentological work. Benthic foraminifers, although consistently rare relative to planktonic species, are the primary facies markers. However, our interpretations are based not only on paleoecologic evidence but include preservational and lithologic criteria as described for deep-water carbonates by Sikora et al. (1999).

Cenozoic Foraminifers

Biostratigraphy for the Cenozoic section employed the planktonic foraminifer zonal time calibration of Berggren et al. (1995). Additional biostratigraphic ranges used are those defined by Kennett and Srinivasan (1983) for the Neogene and by Toumarkine and Luterbacher (1985) and Olsson et al. (1999) for the Paleogene. The paleobathymetric estimates of Van Morkhoven et al. (1986) are followed for deep-water benthic foraminifers.

Mesozoic Foraminifers

The zonal timescale used for the Cretaceous section is that of Gradstein et al. (1995). The Upper Cretaceous biostratigraphic zonation is based upon a combination of that of Caron (1985) and Bergen and Sikora (1999). For the Lower Cretaceous, the zonation of Sliter (1989) is employed. Taxonomy for Lower Cretaceous planktonic foraminifers is that defined by Boudagher-Fadel et al. (1997). Paleobathymetric estimates for the Cretaceous sections follow Nyong and Olsson (1984) and Sikora and Olsson (1991).

Methods

Core catcher samples of ~20 cm^3 (plus one additional sample per section, where necessary) were washed in tap water over a 63-µm mesh sieve to retrieve free specimens of microfossils. More indurated samples were first crushed using a mortar and pestle before washing. Before pro-

cessing each sample, we soaked the sieves in a solution of methylene blue in order to stain any contaminants remaining from previous washes. Washed residues were dried in an oven at ~50°C. We examined the dried samples under a binocular microscope and recorded foraminifer faunal composition in qualitative terms based on an assessment of species observed in a random sample of 200–400 specimens from the >63-µm size fraction. Relative abundances were reported using the following categories:

A = abundant (30%).
C = common (15%–30%).
F = few (3%–15%).
R = rare (2%–3%).
T = trace (<2%).

Preservation of planktonic foraminifer assemblages was recorded as follows:

G = good (<30% of specimens showing signs of dissolution or recrystallization/replacement).
M = moderate (30%–80% of specimens showing signs of dissolution or recrystallization/replacement).
P = poor (>80% of specimens showing signs of dissolution or recrystallization/replacement).

Our relative paleobathymetric estimates use classical continental margin terminology, such as shelf, slope and abyssal, because the paleobathymetric zonations employed were developed from such margins (e.g., Van Morkhoven et al., 1986). The classic paleoenvironmental definition in terms of water depth is employed:

Shelf/slope boundary = 200 m.
Upper/lower slope boundary = 1000 m.
Slope/abyssal boundary = 2000 m.
Deep abyssal = 3000 m.

Although this paleobathymetric scheme varies from the neritic-bathyal-abyssal classification used to describe plateau physiography, we employ it in order to avoid confusion in comparisons to other paleoenvironmental studies. Also, we emphasize that the paleobathymetric zonation used is relative, with water depths given only to define terminology and not intended as absolute values for benthic foraminifer water depth distribution.

We analyzed limestone samples in thin section, oriented across the bedding plane where possible. Identification of microfossils in thin section is primarily based upon the internal and external morphologies of the specimens but also employs wall thickness and structure, test size, and external ornamentation.

IGNEOUS PETROLOGY

Visual Core Descriptions

We used VCD forms to document each section of the igneous rock cores. The left column on the form, adjacent to the core photograph, is

a graphical representation of the archive half. A horizontal line across the entire width of the column denotes a plastic spacer. Oriented pieces are indicated on the form by an upward-pointing arrow in the column to the right. Locations of samples selected for shipboard studies are indicated in the column headed "Shipboard studies" with the following notations:

XRD = X-ray diffraction analysis.
ICP = inductively coupled plasma–atomic emission spectrometry analysis.
TSB = petrographic thin section.
PP = physical properties measurements.
PMAG = paleomagnetic measurements.

Textural and other features documented in the right-hand column use the following notations:

G = unaltered glass.
(G) = altered glass.
SV = sparsely vesicular.
MV = moderately vesicular.
HV = highly vesicular.
X = xenoliths.

Terminology for describing vesicle abundance is defined below (see "Rock Names," p. 13).

After making lithologic descriptions, we subdivided the core into consecutively numbered lithologic units on the basis of changes in structure, brecciation, grain size, vesicle abundance, mineral occurrence and abundance, the presence of sedimentary interbeds, color, and, in some cases, significant changes in drilling rate. Abrupt changes in degree and type of alteration also helped to define some units in massive basalt near the bottom of Hole 1185B. Intercalated sediment horizons were designated as "A" subunits and the underlying volcanic rock as "B" subunits within the same unit. Basaltic breccias or hyaloclastites cemented with carbonate were particularly useful for determining unit boundaries. However, brecciated zones within units were not designated as subunits but simply noted as "brecciated." Although every effort was made to have unit boundaries reflect individual lava packages, the term "unit" should not necessarily be considered synonymous with "lava flow" in this volume.

Rock Names

We assigned provisional rock names based on hand-specimen observations (hand lens and binocular microscope) and later checked them with studies of thin sections. Porphyritic rocks were named by phenocryst type. The term "phenocryst" was used for a crystal that was significantly (typically five times) larger than the average size of the groundmass crystals and generally euhedral in shape. This usage is sensitive to changes in the groundmass grain size (e.g., a single cooling unit could have a moderately phyric aphanitic margin and an aphyric fine-grained interior without any change in the distribution or size of the early-formed crystals). To avoid the problem of describing pillow margins as phyric and cogenetic pillow interiors as aphyric, we based

our terminology on the aphanitic margins of cooling units. If aphanitic pillow margins were sparsely olivine-phyric basalt, we described the fine-grained interiors using the same name even though the euhedral olivine phenocrysts in the pillow interiors were similar in size to groundmass plagioclase laths. Many porphyritic basalts recovered during Leg 192 exhibited a range of groundmass crystal sizes, making estimation of phenocryst populations approximate. We used the following descriptors:

Aphyric: phenocrysts constitute <1% of the volume of the rock.
Sparsely phyric: phenocryst content ranges between 1% and 2%.
Moderately phyric: phenocryst content ranges between >2% and 10%.
Highly phyric: phenocryst content >10%.

We modified these descriptors by including the names of phenocryst phases, in order of decreasing abundance. Thus, a "highly olivine-plagioclase-phyric basalt" contains >10% (by volume) phenocrysts, the dominant phenocryst being olivine, with lesser amounts of plagioclase. The minerals named include all of the phenocryst phases in the rock, as long as the total content >1%. In addition to phenocryst abundance (in volume percent) and size range (in millimeters), we described shape, type and amount of alteration, and made further comments, if appropriate.

Groundmass texture and grain size. Textures are glassy or aphanitic. Grain sizes are fine grained (<1 mm), medium grained (1–5 mm), or coarse grained (>5 mm). We also noted grain size changes within units.

Vesicles. We described vesicles by their abundance, size, and shape (sphericity and angularity). Abundance categories are sparsely vesicular (1–5 vol%), moderately vesicular (>5–20 vol%), and highly vesicular (>20 vol%). Visual estimates of the volume fraction of vesicles were supplemented by observations using a binocular microscope.

Miarolitic cavities. We noted the presence, size, and shape of miarolitic cavities in pillow interiors.

Color name and code. For the dry rock surface, we described color using the Munsell color charts.

Rock structure. Structure is determined by whether the rock is massive, pillowed, hyaloclastic, banded, brecciated, scoriaceous, or tuffaceous. We sought to produce an integrated picture of the style of volcanism and environmental setting of each drill site by identifying features that are diagnostic of specific physical processes. Pillowed sequences were inferred from the presence of glassy margins, groundmass grain-size variations, and vesicle-rich bands. An interval was described as massive if there was no evidence for pillows, even though it may be part of a pillowed sequence. Every effort was made to distinguish brecciated lava from volcaniclastic rocks.

Volcaniclastic rocks contain >60 vol% volcaniclastic grains and <40 vol% biogenic material. This class includes epiclastic rocks (detritus produced by erosion of volcanic rocks by wind or water), pyroclastic deposits (products of explosive magmatism), and hydroclastic rocks (products of granulation by steam [phreatic] explosions and quenching [hyaloclastite and peperite]). For rocks composed of abundant glassy pyroclasts, we followed the classification of Fisher and Schmincke (1984), which uses the names volcanic breccia (clasts >64 mm), lapillistone (>75 vol% lapilli; 2–64 mm), tuff (>75 vol% ash; <2 mm), and lapilli tuff (25–75 vol% lapilli and 25–75 vol% ash). The relative proportions and

types of clasts within the volcaniclastic rocks were recorded and clasts were assigned to the following groups: lithic clasts, vitric clasts, discrete crystal fragments, and matrix (<0.1 mm) or cement. The lithic- to vitric-clast proportions were then used to further classify the rocks (e.g., lithic vitric tuff or vitric lithic tuff). In each case, the second qualifier denotes the more abundant component.

Eruptive style. The features observed were tied to physical processes (e.g., explosive eruption or lava flow), the emplacement style of individual units was inferred (e.g., dominantly pillowed or massive), and the environmental setting for the whole sequence at a site was assessed (e.g., subaerial or submarine).

Alteration. We graded the degree of alteration as unaltered (<2 vol% of alteration products), slight (2–10 vol%), moderate (10–40 vol%), high (40–80 vol%), very high (80–95 vol%), or complete (>95 vol%). We also noted changes of alteration through a section or a unit and briefly described vein abundance, width, mineral linings, and fillings. More detailed descriptions of alteration and weathering of igneous units and of veins and fractures can be found in the "Alteration" and "Structural Geology" sections of each site chapter (see also **"Alteration,"** p. 17, and **"Structural Geology,"** p. 18).

Thin Section Descriptions

We examined thin sections from the core intervals noted on the VCD forms to complement and refine our hand-specimen observations. In general, we used the same terminology for thin section descriptions as for the VCDs. Percentages of individual phases were estimated visually, and textural descriptions were reported (see the **"Core Descriptions"** contents list). The textural terms used are defined by MacKenzie et al. (1982). For some porphyritic basalts, the thin section descriptions and VCDs differ slightly, typically because small plagioclase laths in a rock with seriate texture are visible only in thin section. For example, a rock described in the VCD as olivine-plagioclase-phyric may be plagioclase-olivine-phyric in the thin section description. Similarly, vitric and lithic components may have been estimated incorrectly in volcaniclastic hand samples, and the name assigned may have been different than that determined from a thin section. Where possible, we described at least one thin section per unit.

ICP-AES Analysis

We selected representative samples of major lithologic units for shipboard ICP-AES analysis. Large whole-rock pieces were cut with a diamond-impregnated saw and ground on a diamond wheel to remove surface contamination. We then washed the samples in an ultrasonic bath containing methanol for ~10 min, followed by three consecutive ~10-min washes in an ultrasonic bath containing deionized water. The samples were dried for ~12 hr in an oven at 110°C, after which ~20 cm^3 of each sample was crushed to fragments <1 cm in diameter between two disks of Delrin plastic in a hydraulic press. The chips were ground for ~5 min in a Spex 8510 shatterbox with a tungsten carbide barrel. We weighed the resulting powders on a Scientech balance and ignited them in a furnace at 1100°C for an hour to determine weight loss on ignition (LOI).

We weighed 0.100 ± 0.002-g aliquots of the ignited whole-rock powders and mixed them with 0.4000 ± 0.0004 g of Li metaborate ($LiBO_2$)

flux that had been preweighed onshore. We included standard rock powders and full procedural blanks with the unknowns for each sample run.

Mixtures of flux and rock powders were fused in Pt-Au crucibles at 1050°C for 10–12 min in a Bead Sampler NT-2100. Ten microliters of 0.172-mM aqueous lithium bromide (LiBr) solution was added to the mixture before fusion, as an antiwetting agent to prevent the cooled bead from sticking to the crucible. We transferred the cooled beads to 125-mL polypropylene bottles and dissolved them in 50 mL of 2.3-M HNO_3 by shaking with a Burrell Wrist Action bottle-shaker for an hour. After digestion of the glass bead, all of the solution was filtered to 0.45 µm into a clean 60-mL wide-mouth polypropylene bottle. Next, 2.5 mL of this solution was transferred to a plastic vial and diluted with 17.5 mL of 2.3-M HNO_3 to bring the total volume to 20 mL. The solution-to-sample dilution factor for this procedure is ~4000.

We determined major (Si, Ti, Al, Fe, Mn, Mg, Ca, Na, K, and P) and trace (Zr, Y, Sr, Ba, Ni, Cr, Sc, and V) element concentrations with the JY2000 ULTRACE ICP-AES. The JY2000 sequentially measures characteristic emission intensities (with wavelengths between ~100 and ~800 nm). ICP-AES protocols for shipboard dissolution and analysis of rock powders were developed by Murray et al. (2000) (see also the "Explanatory Notes" chapter of the Leg 187 *Initial Reports* volume [Shipboard Scientific Party, 2001]). We refined the analytical procedure for igneous rocks during Leg 192. All major elements were analyzed in Mode 2 instead of Mode 5 (see below for description). The elements analyzed, emission lines used, and specific analytical conditions used during Leg 192 are provided in Table **T2.** Because of initially poor silica determinations, Si was quantified using three peaks instead of one (for internal verification).

T2. ICP-AES run parameters, p. 46.

The JY2000 plasma was ignited 30 min before each run to allow the instrument to warm up and stabilize. After the warm-up period, a zero-order search was performed to check the mechanical zero of the diffraction grating. After the zero-order search, the mechanical step positions of emission lines were tuned by automatically searching with a 0.002-nm window across each emission peak using the University of Massachusetts Kilauea basalt laboratory standard K-1919, prepared in 2.3-M HNO_3. The only exception is P, which was automatically located by using a single element standard. During the initial setup, we collected an emission profile for each peak, using K-1919, to determine peak-to-background intensities and to set the locations of background points for each element. The JY2000 software uses these background locations to calculate the net intensity for each emission line. We optimized the photomultiplier voltage by automatically adjusting the gain for each element using the standard (BHVO-2, BCR-2, BIR-1, or K-1919) with the highest concentration for that element. During the later part of the leg, the Si peaks were autoattenuated on BHVO-2, even though BCR-2 has a higher Si content, to modify the gain on the Si peaks to increase their intensities. Before each run, we collected a profile of K-1919 to assess the performance of the machine from day to day. A typical sample run lasted ~12–14 hr, depending on the number of samples and replicate analyses.

The parameters for each run are given in Table **T2.** All ICP-AES data presented in the site chapter reports were acquired using Mode 2 of the JY2000 software, except for Fe, Mg, Mn, Ba, Cr, Sc, V, and Y data, which were acquired in Mode 5. In Mode 5, the intensity at the peak of an

emission line is measured and averaged over a given counting interval repeated three times sequentially. Mode 2 fits a Gaussian curve to a variable number of points across a peak and then integrates to determine the area under the curve. We ran each unknown sample at least twice, nonsequentially, in all sample runs.

A typical ICP-AES run includes

1. A set of three certified U.S. Geological Survey (USGS) rock standards (BHVO-2, BIR-1, and BCR-2) (Table T3) run at the beginning, middle, and end of the sample run;
2. Up to 11 unknown samples;
3. A drift-correcting sample (the K-1919 standard) analyzed every fourth sample position; and
4. A blank solution run near the beginning, middle, and end of each run. Also, we ran a 2.3-M HNO_3 wash solution for a minimum of 90 s between each of the samples and standards.

T3. USGS standards values analyzed by ICP-AES, p. 47.

Following each sample run, we transferred the raw intensities to a data file; data reduction was completed using a spreadsheet to ensure proper control over standardization and drift correction. Once transferred, we corrected the intensities for all samples for the full procedural blank. Drift correction was then accomplished by linear interpolation between each consecutively run drift-correcting solution, and corrections to the intensities of the samples run between those drift-correcting solutions were made. We calculated the interpolation using the lever rule. Following blank subtraction and drift correction, we calculated concentrations for each sample from the average intensity per unit concentration for the USGS standard BHVO-2, which was analyzed twice during the run. The resulting major element data were used to calculate the CIPW normative composition (Cross et al., 1903) for each sample.

Estimates of accuracy and precision for major and trace element analyses are based on replicate analyses of BHVO-2, BIR-1, and BCR-2, the results of which are presented in Table T3. In general, run-to-run relative precision by ICP-AES was <2% for the major elements. Run-to-run relative precision for trace elements was generally <5%.

ALTERATION

All igneous rocks recovered during Leg 192 have undergone low-temperature alteration, either halmyrolysis or anoxic alteration. On the hard-rock VCD forms, rocks are graded according to whether they are unaltered (<2 vol% alteration products) or have slight (2–10 vol%), moderate (10–40 vol%), high (40–80 vol%), very high (80–95 vol%), or complete (95–100 vol%) alteration. Alteration and vein/structure core description logs on a piece-by-piece scale were tabulated to provide a consistent characterization of the rocks and to quantify the different alteration types. Descriptions are based mostly on hand-specimen observations of cut wet surfaces; specific clay, zeolite, and carbonate minerals are not generally distinguished, except where crystal morphology allows unequivocal identification. For example, we commonly noted white veins containing only calcium carbonate in the vein/structure logs, although we observed zeolites in some thin sections. When additional mineralogical evidence was available from either thin section descriptions and/or X-ray diffractograms, we integrated these identifications into the alteration logs and the VCDs. However, because of the large

number of veins described, we did not enter thin section and XRD data into the vein/structure log. Table T4 provides a list of abbreviations used in the alteration and vein/structure logs. Bulk rock and halo colors are from the Munsell Soil Color Charts (1975).

We recorded the following information in the alteration and vein/structure logs:

1. The alteration log (Table T5) records bulk-rock alteration. Each entry identifies the igneous unit; the core, section, piece, and interval; the length of each piece; and the depth below the seafloor of the top of each piece. Visual estimates of the alteration type (as represented by rock color and calibrated by thin section observations), the abundance (in percent), size (in millimeters), and mineral fillings of vesicles and miarolitic cavities, and the proportion of altered groundmass and phenocrysts (with the precursor and secondary minerals) are documented for each piece. A column for comments is included.
2. The vein/structure log (Table T6) records the presence, apparent orientation, location, width, and mineral content of veins observed on the cut surface of the core. Each entry identifies the igneous unit and the core, section, piece, and depth below the seafloor of the top of each piece. For each vein, the locations of the top and bottom, depth below the seafloor, mineral fillings and proportions, vein width (in millimeters), and apparent orientation are recorded. We also recorded the presence or absence of a related alteration halo and the color, half width (in millimeters), and alteration mineralogy of halos. A column for comments is included.

T4. Abbreviations in alteration and vein/structure logs, p. 48.

T5. Alteration log form, p. 49.

T6. Vein/structure log form, p. 50.

STRUCTURAL GEOLOGY

The structural features described in the cores recovered during Leg 192 are summarized on the hard-rock VCD forms. For each section, we provided more detailed structural information, such as crosscutting relationships and the apparent and true orientations of veins and fractures, using a separate structural geology description form. These forms are available upon request from the ODP Data Librarian (see the "Related Leg Data" contents list). Structural data are tabulated in the vein/structure logs for each site. The site summary gives more detailed observations. The structural data entered into the vein/structure logs include hole, core, section, piece number, meters below the seafloor for the top of each section, oriented samples (yes or no), and structural identifiers (vein). The data were entered in accordance with a checklist (Table T7).

Veins are indicated as V1…V*n* from the first (top) to the last (bottom) vein. We recorded the interval over which a structural feature occurs on the split core surface. Vein compositions and abbreviations we used are defined in "Alteration," p. 17. Widths of structures are recorded in millimeters. Wall-rock lithology is described by the abbreviations SED (sediment) or BAS (basalt). We determined the orientation of planar features by the values of two apparent-dip measurements, which are used to calculate strike and dip. In addition, we documented the continuity and geometry, thickness, alteration halos, offsets, and crosscutting relationships. We calculated fracture density as number of fractures per meter and vein abundance from vein width as millimeters per meter of core.

T7. Structural geology checklist, p. 51.

PALEOMAGNETISM

Paleomagnetic investigations conducted on the *JOIDES Resolution* during Leg 192 consisted of routine measurements of natural remanent magnetization (NRM) and of magnetic susceptibility of sedimentary and igneous rocks. We measured NRM on all archive split cores of recovered material and on discrete samples of sedimentary and basement rocks taken from the working halves. Stepwise alternating-field (AF) demagnetization was carried out on most archive half cores and on some discrete samples in an attempt to isolate the characteristic remanent magnetization (ChRM). A few discrete samples were thermally demagnetized in order to isolate the ChRM and study the magnetic mineralogy. We measured magnetic susceptibility for whole cores, archive-half core sections, and, in a few cases, discrete samples. We compared magnetic properties with biostratigraphic and lithostratigraphic units.

Laboratory Instruments

We followed the remanence of archive-half sections and oriented discrete samples from working-half sections using a 2-G Enterprises pass-through cryogenic direct-current superconducting quantum interference device rock magnetometer (model 760R). This pass-through cryogenic magnetometer is equipped with an in-line AF demagnetizer (2-G model 2G600) that allows demagnetization of samples up to peak fields of 80 mT. The practical limit on the resolution of natural remanence of core samples is imposed by the magnetization of the core liner itself (~0.01 mA/m). The magnetometer and AF demagnetizer are interfaced to a PC-compatible computer and are controlled by the 2G Long Core software by National Instruments. A Molspin spinner magnetometer was also available on the ship for measuring the remanence of discrete samples. For stepwise demagnetization of discrete samples, the laboratory contains an AF demagnetizer (model D-2000 by DTech Inc.) and a thermal demagnetizer (model TSD-1 by the Schonstedt Instrument Co.) capable of demagnetizing specimens to 200 mT and 700°C, respectively. An Analytical Services Company (ASC) model IM-10 pulse magnetizer (capable of pulsed fields from 0.02 to 1.35 T) and a PARM-2 system by DTech Inc. were available for isothermal and anhysteretic remanent magnetization (IRM and ARM, respectively) acquisition studies of discrete samples.

We measured magnetic susceptibility for all whole-core sections at 4-cm intervals with a susceptibility meter attached to the MST (see **"Physical Properties,"** p. 21). The susceptibility values were stored in the Janus database as raw data in units of 10^{-5} SI. The true SI volume of susceptibilities should be multiplied by a correction factor to account for the volume of material that passed through the coils. The standard correction factor for ODP core is ~0.66. We routinely measured the magnetic susceptibility of archive halves of sediment cores using the AMST (see **"Lithostratigraphy,"** p. 6) at 4-cm intervals. Some archive halves were measured using a 2-cm interval. The AMST, which permits measurements only at evenly spaced intervals along each section of core, automatically recorded the measurements. For the two types of susceptibility measurements (MST and AMST), we used the same type of magnetic susceptibility meter (Bartington Instruments model MS2) but with a different sensor. The sensor for whole-core measurements (MS2C) has an 80-mm inner diameter, and the core passes through the

sensor coil. The AMST has a cylindrical tip probe (MS2F), and the sensor provides a depth of investigation approximately equal to its diameter (20 mm). A Geofyzika Brno Kappabridge KLY-2 magnetic susceptibility meter was available for magnetic susceptibility measurements of discrete samples.

Sampling Coordinates

We followed the standard ODP core orientation convention (Shipboard Scientific Party, 1991 [fig. 8], and 1997 [fig. 8]) for paleomagnetic work during Leg 192. This convention can be described as follows. The z-axis is downhole parallel to the core. The x-axis forms a line perpendicular to the split face of the core and is directed into the working half (Fig. F6). The x-axis is used as the reference "geomagnetic north" for the definition of magnetic declination values. Discrete sample cubes and minicores were marked with an arrow in the negative-z (uphole) direction on the plane representing the split surface of the working half. The plane marked with the arrow is the y-z plane. Because only the rotary core barrel (RCB) was used for drilling, we were unable to use the Tensor tool, which mounts on the advanced hydraulic piston corer (APC) core barrel to orient cores.

F6. Coordinate systems of ODP cores and samples, p. 42.

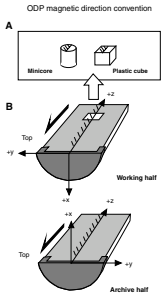

Sampling Method

Discrete samples were taken from soft sediment using standard plastic cubes (7 cm^3), with an arrow pointing in the uphole direction. We did not take samples from portions of the core that were highly disturbed by drilling. To reduce deformation of the sediment while pressing in the plastic cubes, we cut the core with a thin stainless steel spatula before pressing the cubes into the sediment. Cylindrical minicores (12 cm^3) were drilled from hard sediment and igneous rocks using a water-cooled nonmagnetic drill bit attached to a standard drill press. Minicores were oriented in the same manner, with an arrow pointing in the uphole direction. We typically took discrete samples at an increment of one or two per core, and some were used for onboard pilot demagnetization studies. However, some discrete samples were taken from sedimentary rocks at smaller increments to examine geomagnetic reversals, key geologic boundaries, or other intervals of interest. Several discrete samples per flow unit were taken from igneous rocks.

Measurements

We analyzed the NRM of the archive-half sections on the cryogenic magnetometer at 5-cm intervals for sedimentary material and at 1-cm intervals for igneous rocks when continuous pieces longer than 15 cm were available. To isolate characteristic magnetizations, archive halves were AF demagnetized at 5, 10, and 15 mT for sediments. Basalt samples were generally stepwise AF demagnetized up to 50 mT: a few samples were demagnetized to 80 mT. The number of demagnetization steps and the peak field used varied depending on the lithology, the NRM intensity, and the amount of time available. To isolate stable remanence, we applied stepwise thermal demagnetization of up to 620°C to some discrete samples of the volcaniclastic rocks. We performed some IRM acquisition experiments on sediments to define their dominant magnetic mineralogy.

Analysis

We obtained the characteristic remanent magnetizations of both sediment and basalt samples using principal-component analysis (Kirschvink, 1980) on the results of the AF demagnetization. We determined the stability of remanence levels within the archive cores and the discrete samples by both Zidjerveld (1967) plots and equal-area stereographic projections.

Magnetozones were defined by selected directional data from the cryogenic magnetometer. Typical selection criteria were as follows:

1. Intensity of NRM after AF demagnetization at 15 mT stronger than 2×10^{-4} A/m and hence above the noise level of the magnetometer in a condition of rough sea,
2. Inclination >+10° or <–10°,
3. At least three consecutive values (which corresponds to a minimum of 10-cm length of split core) of the same polarity, and
4. No significant core disturbance.

Positive and negative inclinations were defined as reversed and normal magnetic polarities, respectively. We then interpreted the magnetic polarity stratigraphy using constraints from the biostratigraphic data (see **"Biostratigraphy,"** p. 10). We used the timescales of Berggren et al. (1995) for the Cenozoic polarity boundaries and Gradstein et al. (1995) (see **"Biostratigraphy,"** p. 10) for the Mesozoic polarity boundaries.

We calculated mean inclination values at each site using the method of Kono (1980). These inclinations were used to obtain paleolatitudes based on the assumption of an axial dipole field using the equation

$$\tan(\text{paleolatitude}) = \tfrac{1}{2}\tan(\text{inclination}). \quad (2)$$

We compared the results from the remanent magnetization and low-field susceptibility measurements with lithologic units and/or geologic structures based on sedimentary, petrologic, and structural features (see **"Lithostratigraphy,"** p. 6, **"Igneous Petrology,"** p. 12, and **"Structural Geology,"** p. 18).

PHYSICAL PROPERTIES

Introduction and General Objectives

Shipboard physical properties determinations may be correlated with core lithology, downhole geophysical results, and regional seismic data. The principal objectives of the physical properties measurement program were as follows:

1. Provide comprehensive data sets of density, porosity, thermal conductivity, magnetic susceptibility, and sonic velocity variations.
2. Integrate physical properties data obtained from the cores with physical parameters derived from downhole logging. Parameters such as bulk density, porosity, and sonic velocity can aid log interpretation.

3. Help identify the occurrence of fine-scale depositional events. Magnetic susceptibility spikes, for example, can be used to identify thin ash layers.
4. Assist in the interpretation of geophysical survey data. For example, sonic velocity data corrected to in situ values using a depth-based function (Urmos et al., 1993) can facilitate the interpretation of seismic reflection profiles.

We measured physical properties on unsplit cores and on the undisturbed parts of split cores. We used the MST for nondestructive measurements of wet bulk density, compressional wave velocity, magnetic susceptibility, and natural gamma radiation in unsplit cores. Thermal conductivity was measured on unsplit soft-sediment cores and split lithified sediment and hard-rock cores and three-directional compressional wave (*P*-wave) velocities on both soft- and hard-rock cores. Portions of split cores that were undisturbed by drilling provided specimens for measurement and calculation of index properties (wet bulk density, grain density, dry bulk density, water content, void ratio, and porosity).

Measurements were made after cores had been allowed to stand for 2–4 hr to equilibrate approximately to ambient room temperature (i.e., 22°–24°C). All instruments and apparatuses used in the shipboard laboratory and the principles of the methods employed were described by Blum (1997). Below, we summarize each type of physical properties measurement made during Leg 192.

Multisensor Track Measurements

The MST includes four physical properties sensors (magnetic susceptibility meter, gamma ray attenuation (GRA) densitometer, *P*-wave logger, and natural gamma radiation detector). We placed individual, unsplit core sections on the MST, which automatically moves the section through the sensors on a fiberglass track. MST data were taken at discrete intervals chosen to optimize data resolution within the time limitations of running each core section through the device.

Magnetic Susceptibility Measurement

We determined magnetic susceptibility on all sections at 4-cm intervals using the 1.0 (1 s integration time) range on the Bartington meter (model MS2C), which has an 88-mm coil diameter. The MS2C meter measures relative susceptibilities, which are not corrected for the difference between core and coil diameters. Magnetic susceptibility helps detect variations in magnetic properties caused by lithologic changes or alteration. The quality of the data is degraded in RCB sections if the core liner is not completely filled or the core is disturbed. However, general downhole trends may still be used for correlation with well logs. During Leg 192, we also measured magnetic susceptibility with a point susceptibility meter on the AMST. We routinely compared data from the two instruments.

Gamma Ray Attenuation Densitometer

Bulk density was estimated for unsplit core sections as they passed through the GRA densitometer using a sampling period of 2 s every 4 cm on the MST. The gamma ray source was ^{137}Cs. For each site, we com-

pared the bulk density obtained from the densitometer and the bulk densities measured on discrete samples. GRA bulk density data are most reliable in undisturbed cores and offer the potential of direct correlation with downhole bulk density logs. We did not acquire GRA bulk density data on highly fragmented cores. Where cores were not filling the liners or were disturbed or fractured, we expect the GRA density to be generally lower.

Compressional Wave Logger

The *P*-wave logger (PWL) operates simultaneously with the GRA and transmits a 500-kHz compressional wave pulse through the core at a frequency of 1 kHz. A pair of displacement transducers monitors the separation between the *P*-wave transducers. Data are collected at 4-cm intervals. MST measurement of *P*-wave velocities typically is not possible on RCB cores because of the loss of coupling between the liner and the core and thus was not done on most of the Leg 192 cores.

Natural Gamma Radiation Detector

Measurement of natural gamma radiation depends on the random and discrete decay of radioactive atoms and is measured with scintillation detectors as outlined by Hoppie et al. (1994). During Leg 192 we measured natural gamma radiation (NGR) every 4-cm length of core. Results were output in counts per second. The NGR detector system was calibrated in port against a thorium source, and sample standards were measured at the end of operations at every site.

Thermal Conductivity

Thermal conductivity is the rate at which heat is transmitted by molecular conduction. It is an intrinsic material property that depends on the chemical composition, porosity, density, structure, and fabric of the material. Thermal conductivity profiles of sediment and rock sections are used mainly, along with temperature measurements, to calculate heat flow. Heat flow is not only characteristic of the material but also helps to indicate the age of ocean crust and fluid circulation processes at a range of depths (e.g., Blum, 1997). During Leg 192, we used the TK04 (TeKa, Berlin) system to acquire thermal conductivity data. This system employs a continuously heated single-needle probe (von Herzen and Maxwell, 1959) used in full-space configuration for soft sediments and in half-space mode for lithified sediment and hard-rock samples. We typically acquired data for every core. The thermal conductivity value reported for each sample is the average of three (full-space method) or four (half-space method) repeated measurements. Data are reported in units of watts per meter per degree kelvin (W/[m·K]).

Soft-Sediment Full-Space Determinations

Full cores of unconsolidated sediment were measured for thermal conductivity by inserting a full-space single-needle probe (containing a heater wire and a calibrated thermistor) into the sediment through a small hole drilled in the core liner before the sections were split. Temperatures, recorded for times between 60 and 240 s, were fitted to the following equation using the least-squares method (von Herzen and Maxwell, 1959):

$$T(t) = (q/4\pi k) \cdot \ln(t) + L(t), \quad (3)$$

where

T = temperature (°C),
q = heat input per unit length of wire (W/m)
k = apparent thermal conductivity (W/[m·K]), and
t = time (s).

The term $L(t)$ corrects for temperature drift, as described in the following equation:

$$L(t) = At + T_e, \quad (4)$$

where A represents the rate of temperature change and T_e is the equilibrium temperature. $L(t)$ therefore corrects for the background temperature drift, systematic instrumental errors, probe response, and sample geometry. The best fit to the data determines the values of k and A.

Lithified Sediment and Hard-Rock Half-Space Determinations

We made half-space determinations on selected lithified sediments and basaltic rock samples after the cores were split and their faces were polished. The half-space needle probe was secured to the polished face. The needle probe rested between the polished surface and a grooved epoxy block with relatively low thermal conductivity (Sass et al., 1984; Vacquier, 1985). We conducted half-space measurements in a water bath to keep the samples saturated, to improve the thermal contact between the needle and the sample, and to reduce thermal drift. Data collection and reduction procedures for half-space tests are similar to those for full-space tests except for a multiplicative constant in Equation 4 that accounts for the different experimental geometry.

Index Properties Measurements

We extracted one ~10-cm³ sample from each section of freshly cut core to determine index properties. We calculated bulk density, grain density, water content, porosity, and dry density from wet and dry sample mass and dry volumes. Sample mass was determined using two Scitech electronic balances equipped with a computerized averaging system that corrected for ship accelerations. The sample mass was counterbalanced by a known mass, such that the mass differentials generally were <1 g. Using a helium-displacement Quantachrome Penta-Pycnometer, we determined sample volumes at least three times, until consistent readings were obtained. A standard reference volume was included with each group of samples during the measurements and rotated among the cells to check for instrument drift and systematic error. After the samples were oven dried at 105° ± 5°C for 24 hr and allowed to cool in a desiccator, we measured dry weights and volumes (method C of Blum, 1997). The following relationships were computed from two mass measurements and dry volume measurements (taken from Blum, 1997, pp. 2-2 to 2-3). First, we subtracted the beaker mass and volume (determined periodically and stored in the program's "look-up" table)

from the measured total mass and volume, yielding the following directly measured values:

M_b = bulk mass.
M_d = dry mass (mass of solids [M_s] + mass of residual salt).
V_d = dry volume (volume of solids [V_s] + volume of evaporated salt [V_{salt}]).

Variations in pore-water salinity (s) and density (ρ_{pw}) that typically occur in marine sediments do not affect the calculations significantly, and standard seawater values at laboratory conditions (Boyce, 1976) are used:

s = 0.035 and
ρ_{pw} = 1.024 g/cm³.

Pore-water mass (M_{pw}), mass of solids (M_s), and pore-water volume (V_{pw}) are then calculated as follows:

$$M_{pw} = (M_b - M_d)/(1 - s), \quad (5)$$

$$M_s = M_b - M_{pw} = (M_d - s\,M_b)/(1 - s), \text{ and} \quad (6)$$

$$V_{pw} = M_{pw}/\rho_{pw} = (M_b - M_d)/(1 - s)\rho_{pw}. \quad (7)$$

To account for the phase change of pore-water salt during drying, the mass and volume of salt (M_{salt} and V_{salt}, respectively) are required. For practical purposes, the mass of salt is the same in solution and as a precipitate, whereas the volume of the salt in solution is negligible.

$$M_{salt} = M_{pw} - (M_b - M_d) = (M_b - M_d)s/(1 - s) \text{ and} \quad (8)$$

$$V_{salt} = M_{salt}/\rho_{salt} = [(M_b - M_d)s/(1 - s)]/\rho_{salt}, \quad (9)$$

where the salt density ρ_{salt} = 2.20 g/cm³ is calculated for average sea salt. Moisture content is the pore-water mass expressed either as percentage of wet bulk mass (W_b) or as percentage of the mass of salt-corrected solids (W_s):

$$W_b = M_{pw}/M_b = (M_b - M_d)/[M_b(1 - s)] \text{ or} \quad (10)$$

$$W_s = M_{pw}/M_s = (M_b - M_d)/(M_d - sM_b). \quad (11)$$

Calculation of the volume of solids and bulk volume is as follows:

$$V_s = V_d - V_{salt} \text{ and} \quad (12)$$

$$V_b = V_s + V_{pw}. \quad (13)$$

Bulk density (ρ_b), density of solids or grain density (ρ_s), dry density (ρ_d), porosity (P), and void ratio (e) are then calculated according to the following equations:

$$\rho_b = M_b/V_b, \quad (14)$$

$$\rho_s = M_s/V_s, \quad (15)$$

$$\rho_d = M_s/V_b, \quad (16)$$

$$P = V_{pw}/V_b, \text{ and} \quad (17)$$

$$e = V_{pw}/V_s. \quad (18)$$

Sonic Velocity Determinations

For discrete *P*-wave velocity measurements in split cores, we used the PWS3 contact probe system with a signal frequency of 500 kHz. We measured *P*-wave velocity (500 kHz) once or twice per section and in more than one direction of the core where possible. Distilled water constituted the coupling fluid at the transducer/core interface. Sediments were measured in half liners or in discrete samples taken from the core. We sampled crystalline and basaltic rocks as minicores (2.54 cm in diameter) drilled perpendicular to the axis of the core (x-direction) or sawed as oriented cubes. The ends of the minicores were trimmed parallel to each other with a rock saw, and we measured traveltimes and distances along the axis of the minicore. For cubes, velocities were determined in two or three mutually perpendicular directions, V_z (along the core), V_x (into the split core, perpendicular to core axis), and V_y (across the split core). Velocity anisotropy follows the relationship

$$\text{Anisotropy} = 3(V_{max} - V_{min})/(V_x + V_y + V_z), \quad (19)$$

where V_{max} and V_{min} are the maximum and minimum velocities among V_x, V_y, and V_z. During Leg 192 we made velocity determinations either adjacent to paleomagnetic minicores or directly on the minicores to save core material. We calculated velocities using the corrected traveltime and path length. Velocity data are reported in raw form. In intervals where discrete sampling was sparse and if time allowed, we made additional measurements on split pieces of hard rocks. Velocities from these measurements may have slightly lower values because the contact surface tended to be comparatively irregular. Nevertheless, velocities determined from hard-rock pieces should exhibit downhole trends similar to those determined from discrete samples.

DOWNHOLE MEASUREMENTS

Introduction

Downhole logs are continuous records of the in situ physical properties of the formation penetrated by a borehole. The logs are made using a variety of sensors, called sondes, which are stacked together in combinations known as tool strings. These are lowered down the hole on a heave-compensated electrical wireline and then pulled up at constant speed while acquiring data from which many properties can be determined as a function of depth.

Log data are used to interpret formation structure, stratigraphy, lithology and mineralogy. Where core recovery is incomplete or disturbed, log data may provide the only way to characterize the borehole section. Where core recovery is good, log and core data complement

one another and Formation MicroScanner (FMS) images may be used for core orientation. Synthetic seismograms constructed from borehole sonic data provide the best-known method for traveltime-to-depth conversion of surface seismic data. Finally, downhole logs are sensitive to formation properties on scales that are intermediate between those of laboratory measurements on core samples and those of surface geophysical surveys. They therefore provide a necessary link in the integrated understanding of physical properties on all scales.

Tool Strings

Two combinations of downhole sensors were used during Leg 192: the geophysical tool string and the FMS/sonic tool string (Fig. F7). With the exception of the Lamont-Doherty high-resolution temperature/acceleration/pressure (TAP) tool, the tool strings used during Leg 192 were made up exclusively of Schlumberger sondes.

The geophysical tool string (Fig. F7) measures formation electrical resistivity, density, porosity, and radioactivity, and is therefore also known as the "quad combo." The tools that make up this string are the accelerator porosity sonde (APS), the hostile-environment natural gamma ray sonde (HNGS), the hostile-environment lithodensity sonde (HLDS), and the phasor dual induction–spherically focused resistivity tool (DITE-SFR). The TAP tool was attached to the bottom of the Schlumberger tool string.

The FMS/sonic tool string (Fig. F7) provides electrical images of the borehole walls and determines acoustic velocity in the formation and the downhole magnetic field vector. The tools that make up this string are the FMS logging tool (Fig. F8), the general-purpose inclinometer (three-axis magnetometer-inclinometer) tool (GPIT), and the dipole shear sonic imager (DSI). The natural gamma spectrometry tool (NGT), which measures radioactivity, was included in this tool string.

Each tool string includes a telemetry cartridge for communicating through the wireline with the logging laboratory on the drillship and a natural gamma ray (NGR) sonde that identifies lithologic markers, providing a common reference for depth-matching between multiple logging runs.

The logging tools, their operating principles, log applications, and factors affecting data quality are briefly described below. Principal data channels of the tools, their physical significance, and units of measurement are listed in Table T8. The logging speeds used during Leg 192, properties of the formation determined by each tool, measurement sampling intervals, approximate vertical resolutions, and depths of investigation are summarized in Table T9. More detailed information on individual tools and their geological applications may be found in Ellis (1987), Goldberg (1997), Hearst and Nelson (1984), Rider (1996), Schlumberger (1989, 1994), Serra (1984, 1986, 1989), and on the Lamont-Doherty Borehole Research Group Web site (see the "Related Leg Data" contents list).

Natural Radioactivity

We used two spectral gamma ray tools to measure natural radioactivity in the formation: the NGT and the HNGS. The NGT uses a sodium iodide scintillation detector and five-window spectrometry to determine concentrations of potassium, thorium, and uranium, the three elements whose isotopes dominate the natural radiation spectrum. The

F7. Tool strings used during Leg 192, p. 43.

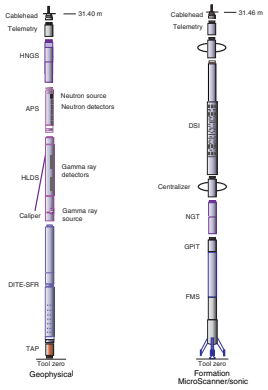

F8. Diagram of the FMS pad, p. 44.

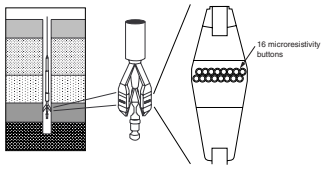

T8. Tool and measurement acronyms, p. 52.

T9. Logging tools specifications, p. 53.

HNGS is similar to the NGT, but it uses two bismuth germanate scintillation detectors and 256-window spectrometry for significantly improved tool precision. The hostile-environment natural gamma ray sonde derives its name from the fact that it is rated to a much higher temperature (260°C) than the natural gamma spectrometry tool (149°C).

The gamma ray log is one of the few that provides useful data in cased wells. It is therefore used as a correlation curve for depth matching between individual logging runs, with lithologic markers or the seafloor acting as reference points. Gamma ray logs may also be used for clay typing, mineralogy, and ash-layer detection. Clean sedimentary formations usually have a very low level of radioactivity. Potassium and thorium tend to concentrate in clays and shales. An increase of potassium in carbonates can be related to either the presence of algal material or glauconite, whereas the presence of uranium is often more closely associated with organic matter. Thorium is commonly found in ash layers.

Because the natural gamma ray response is sensitive to borehole diameter and the weight and concentration of bentonite or potassium chloride present in the drilling mud, corrections are routinely made for these effects during data processing by the Borehole Research Group at Lamont-Doherty Earth Observatory.

Density

We determined formation density from gamma ray attenuation with the hostile-environment lithodensity sonde. The sonde contains a radioactive cesium (^{137}Cs) gamma ray source (622 keV) and far and near gamma ray detectors mounted on a shielded skid that is pressed against the borehole wall by a hydraulically activated arm. Gamma rays emitted by the source experience Compton scattering, which involves the transfer of energy from gamma rays to electrons in the formation via elastic collision. The number of scattered gamma rays that reach the detectors is related to the density of electrons in the formation, which is, in turn, related to bulk density. Porosity may be derived from this bulk density if the matrix density is known.

The HLDS also measures the photoelectric effect factor (PEF) caused by absorption of low-energy gamma rays. Photoelectric absorption occurs when gamma rays reach energies of <150 keV after being repeatedly scattered by electrons in the formation. Because photoelectric absorption depends strongly on the mean atomic number of the elements in the formation, it varies according to chemical composition and is essentially independent of porosity. For example, the PEF of pure calcite = 5.08 barn/electron, illite = 3.03 barn/electron, quartz =1.81 barn/electron, and kaolinite = 1.49 barn/electron. PEF values can therefore give an indication of the chemical composition of the formation and can be used in combination with natural gamma ray data to identify different clay minerals.

Porosity

Formation porosity was determined using the accelerator porosity sonde. The sonde incorporates a minitron neutron generator which produces fast (14.4 MeV) neutrons. Five neutron detectors (four epithermal and one thermal) measure the number and arrival times of neutrons at different distances from the source. Neutrons emitted from the source

are slowed by collisions with nuclei in the formation, experiencing an energy loss that depends on the relative mass of the nuclei with which the neutrons collide. Maximum energy loss occurs when a neutron strikes a hydrogen nucleus. As hydrogen is mainly present in pore water, the neutron log essentially measures porosity, assuming pore-fluid saturation. However, as clays and hydrocarbons also contain hydrogen, the log often overestimates raw porosity and the results should be treated with caution.

Electrical Resistivity

The electrical resistivity of the formation was measured with the phasor dual induction–spherically focused resistivity tool. This sonde provides three measures of electrical resistivity based on different depths of investigation: shallow, medium, and deep (Table T9). Shallow-penetration measurements with a high vertical resolution are made with a spherically focused laterolog. This is a constant-current device that uses bucking electrodes to focus the path taken by the measurement current in the formation. Medium- and deep-penetration measurements are made inductively using transmitter coils energized with high-frequency alternating currents, creating time-varying magnetic fields that induce secondary Foucault currents in the formation. The strength of the induced ground currents is inversely proportional to the resistivity of the formation through which they circulate, as are the secondary inductive fields that they create. Formation resistivity is deduced from the amplitude and phase of the secondary magnetic fields, which are measured with receiving coils.

Induction sondes are most accurate in low- to medium-resistivity formations (<100 Ωm), whereas focused continuous-current devices such as the Schlumberger Dual Laterolog (DLL) are preferable for measurements in resistive basalts. As the greater part of the logged interval was in sediments during Leg 192, the dual induction tool was selected over the DLL to measure electrical resistivity.

The solid constituents of crustal rocks are highly resistive relative to the pore fluids. Electricity is conducted primarily by ion transport through pore fluids, and electrical conductivity strongly depends on porosity and pore connectivity. Electrical resistivity data can accordingly be used to estimate formation porosity using Archie's Law (Archie, 1942) if the formation does not contain clay. Archie's Law is expressed as $FF = a\,\phi^{-m}$, where FF is the formation factor (the ratio of the formation resistivity to that of the pore fluids); ϕ is the porosity; m is known as the cementation factor and depends on the tortuosity and connectivity of pore spaces; and a is a constant that varies with rock type.

Temperature, Acceleration, and Pressure

Downhole temperature, acceleration, and pressure were measured with the Lamont-Doherty high-resolution temperature/acceleration/pressure tool. Attached to the bottom of the geophysical tool string, this sonde operates in an autonomous mode, with data stored in built-in memory. A two-component thermistor (for different temperature ranges) is mounted near the bottom of the tool in a slotted protective cover. The time constant of the thermistor assembly in water is ~0.4 s. The tool also includes a pressure transducer (0–10,000 psi), which is used to activate the tool at a specified depth and to measure pressure, and a high-sensitivity vertical accelerometer, which provides data for

analyzing the effects of heave on a deployed tool string. Temperature and pressure data are recorded once per second, and accelerometer data can be recorded at a 4- or 8-Hz sampling rate.

The temperature record must be interpreted with caution, as the amount of time elapsed between the end of drilling and the logging operation is generally not sufficient to allow the borehole to recover thermally from the influence of cold drilling fluid circulation. The temperature profile recorded under such circumstances may differ significantly from that of the surrounding formation. Nevertheless, abrupt changes in the temperature gradient can indicate regions of fluid entrainment in, or inflow from, permeable layers. In cases where the borehole has thermally reequilibrated with the surrounding formation, we can determine vertical heat flow from the temperature gradient combined with measurements of thermal conductivity on core samples.

Acoustic Measurements

The dipole shear sonic imager employs a combination of monopole and dipole transducers to make accurate measurements of sonic wave propagation in a wide variety of lithologies. The DSI measures the transit times between sonic transducers and an array of eight receivers. Along with the monopole transducers found on most sonic tools, the DSI has two crossed dipole transducers. These allow the determination of shear and Stoneley wave velocities in addition to compressional wave velocity, even in the seismically slow formations commonly encountered in ODP boreholes.

Data from the DSI are used to generate synthetic seismograms for traveltime-to-depth conversions of surface seismic data.

Magnetic Field Measurement

Downhole magnetic field measurements were made with the general purpose inclinometer tool. The primary purpose of this sonde, which incorporates a three-component accelerometer and a three-component magnetometer, is to determine the acceleration and orientation of the FMS during logging. The acceleration data allow more precise determination of log depths than is possible on the basis of cable length alone, as the wireline is subject to both stretching and ship heave. Acceleration data are also used in processing FMS data to correct the images for irregular tool motion.

Local magnetic anomalies, generated by high remanent magnetization of basalts in the basement section of a borehole, can interfere with the determination of tool orientation. However, these magnetic anomalies are frequently used to infer the magnetic stratigraphy of the basement section.

Formation MicroScanner

The FMS provides high-resolution, electrical-resistivity-based images of borehole walls. The tool has four orthogonal arms (pads), each containing 16 microelectrodes known as "buttons," which are pressed against the borehole wall during the recording. The electrodes are arranged in two diagonally offset rows of eight electrodes each and are spaced ~2.5 mm apart. A focused current is emitted from the four pads into the formation, with a return electrode near the top of the tool. Array buttons on each of the pads measure the current intensity varia-

tions. Processing transforms these measurements of the microresistivity variations of the formation into continuous, spatially oriented high-resolution images that mimic geologic structures behind the borehole walls. Further processing can provide the dip and direction (azimuth) of planar features in the formation. FMS images are particularly useful for mapping structural features, dip determination, detailed core-log correlation, positioning of core sections with poor recovery, and analysis of depositional environments.

The FMS image is sensitive to structure within ~25 cm of the borehole wall and has a vertical resolution of 5 mm with a coverage of 22% of the borehole wall on a given pass. FMS logging commonly includes two passes, the images of which are merged to improve borehole wall coverage.

To produce reliable FMS images, the pads must be firmly pressed against the borehole wall. The maximum extension of the caliper arms is 38 cm (15 in). In holes with a diameter larger than this, the pad contact is inconsistent and the images are blurred. Irregular borehole walls also adversely affect the images as contact with the wall is poor.

Log Data Quality

The quality of log data may be seriously degraded by excessively wide sections of the borehole or by rapid changes in the hole diameter. Resistivity and velocity data are the least sensitive to borehole effects, whereas nuclear measurements (density, neutron porosity, and both natural and induced spectral gamma rays) are most sensitive because of the large attenuation by borehole fluid. Corrections can be applied to the original data to reduce the effects of most borehole conditions that depart from those under which the tool was calibrated.

Logs from different tool strings may have depth mismatches caused by either cable stretch or ship heave during recording. Small errors in depth matching can distort the logging results in zones of rapidly changing lithology. To minimize the effects of ship heave, a hydraulic wireline heave compensator adjusts for rig motion during logging operations. Distinctive features recorded by natural gamma ray tools, included on every tool string, provide correlation and relative depth offsets between logging runs and can be calibrated to distinctive lithologic contacts observed in the recovered core or during drilling operations (e.g., basement contacts).

Data Recording and Processing

Data for each logging run are recorded, stored digitally, and monitored in real time using the Schlumberger multitasking acquisition and imaging system (MAXIS 500). On completion of logging at each hole, data are transferred to the shipboard downhole measurements laboratory for preliminary interpretation. FMS image data are processed onboard using Schlumberger GeoQuest's "Geoframe" software package.

Additional processing of the logs is carried out onshore by the Borehole Research Group at Lamont-Doherty Earth Observatory, after the data are transmitted by satellite from the ship. It includes adjustments to remove depth offsets between data from different logging runs; corrections for borehole conditions specific to certain tools and logs; documentation for the logs, with an assessment of log quality; and conversion of the data to a widely accessible format (ASCII for the conven-

tional logs and GIF for FMS images). Schlumberger GeoQuest's "GeoFrame" software package is used for most of the processing.

Processed acoustic, caliper, density, gamma ray, magnetic, neutron porosity, resistivity, and temperature data in ASCII format are available at the Lamont-Doherty Borehole Research Group Web site (see the **"Related Leg Data"** contents list). A summary of logging highlights is also posted on the BRG Web site.

REFERENCES

Araki, E., Mochizuki, K., Suyehiro, K., Taira, A., Yoneshima, S., Shinohara, M., Miura, S., and Hino, R., 1998. Seismic structure of Ontong Java Plateau crust, *Eos, Trans. Am. Geophys. Union,* 79, F869.

Archie, G.E., 1942. The electrical resistivity log as an aid in determining some reservoir characteristics. *J. Pet. Technol.,* 5:1–8.

Balsam,W.L., and Damuth, J.E., 2000. Further investigations of shipboard vs. shore-based spectral data: implications for interpreting Leg 164 sediment composition. *In* Paull, C.K., Matsumoto, R., Wallace, P., and Dillon, W.P. (Eds.), *Proc. ODP, Init. Repts.,* 164: College Station, TX (Ocean Drilling Program), 313–324.

Balsam, W.L., Damuth, J.E., and Schneider, R.R., 1997. Comparison of shipboard vs. shore-based spectral data from Amazon-Fan cores: implications for interpreting sediment composition. *In* Flood, R.D., Piper, D.J.W., Klaus, A., and Peterson, L.C. (Eds.), *Proc. ODP, Sci. Results,* 155: College Station, TX (Ocean Drilling Program), 193–215.

Balsam, W.L., Deaton, B.C., and Damuth, J.E., 1998. The effects of water content on diffuse reflectance measurements of deep-sea core samples: an example from ODP Leg 164 sediments. *Mar. Geol.,* 149:177–189.

Bergen, J.A., 1998. Calcareous nannofossils from the lower Aptian historical stratotype as Cassis-La Bedoule. *Geol. Medit.,* no. 3/4:227–255.

Bergen, J.A., and Sikora, P., 1999. Microfossil diachronism in southern Norwegian North Sea chalks: Valhall and Hod Field. *In* Jones, R.W., and Simmons, M.D. (Eds.) *Biostratigraphy in Production and Development Geology.* Spec. Publ.—Geol. Soc. London, 152:85–111.

Berggren, W.A., Kent, D.V., Swisher, C.C., III, and Aubry, M.-P., 1995. A revised Cenozoic geochronology and chronostratigraphy. *In* Berggren, W.A., Kent, D.V., Aubry, M.-P., and Hardenbol, J. (Eds.), *Geochronology, Time Scales and Global Stratigraphic Correlation.* Spec. Publ.—Soc. Econ. Paleontol. Mineral. (Soc. Sediment. Geol.), 54:129–212.

Blum, P., 1997. Physical properties handbook: a guide to the shipboard measurement of physical properties of deep-sea cores. *ODP Tech. Note,* 26 [Online]. Available from World Wide Web: <http://www-odp.tamu.edu/publications/tnotes/tn26/INDEX.HTM>. [Cited 2000-09-08]

Boudagher-Fadel, M.K., Banner, F.T., and Whittaker, J.E., 1997. *The Early Evolutionary History of Planktonic Foraminifers:* Br. Micropal. Soc. Publ. Series: London (Chapman & Hall).

Bown, P.R. (Ed.), 1998. *Calcareous Nannofossil Biostratigraphy:* London (Kluwer Academic).

Boyce, R.E., 1976. Definitions and laboratory techniques of compressional sound velocity parameters and wet-water content, wet-bulk density, and porosity parameters by gravimetric and gamma-ray attenuation techniques. *In* Schlanger, S.O., Jackson, E.D., et al., *Init. Repts. DSDP,* 33: Washington (U.S. Govt. Printing Office), 931–958.

Bralower, T.J., Leckie, R.M., Sliter, W.V., and Thierstein, H.R., 1995. An integrated Cretaceous microfossil biostratigraphy. *In* Scholle, P.A. (Ed.), *Geochronology, Time Scales, and Global Stratigraphic Correlation.* Spec. Publ.—Soc. Econ. Paleontol. Mineral. (Soc. Sediment. Geol.), 54:65–79.

Bralower, T.J., Sliter, W.V., Arthur, M.A., Leckie, R.M., Allard, D.J., and Schlanger, S.O., 1993. Dysoxic/anoxic episodes in the Aptian-Albian (Early Cretaceous). *In* Pringle, M.S., Sager, W.W., Sliter, M.V., and Stein, S. (Eds.), *The Mesozoic Pacific: Geology, Tectonics, and Volcanism.* Geophys. Monogr., Am. Geophys. Union, 77:5–37.

Burnett, J.A., 1997. New species and conjectured evolutionary trends of *Ceratolithoides* from the Campanian and Maastrichtian of the Indian Ocean. *J. Nannoplankton Res.,* 19/2:123–131.

Caron, M., 1985. Cretaceous planktic foraminifera. *In* Bolli, H.M., Saunders, J.B., and Perch-Nielsen, K. (Eds), *Plankton Stratigraphy:* Cambridge (Cambridge Univ. Press), 17–86.

Cross, W., Iddings, J.P., Pirsson, L.V., and Washington, M.S., 1903. *Quantitative Classification of Igneous Rocks:* Chicago (Univ. Chicago Press).

Dunham, R.J., 1962. Classification of carbonate rocks according to depositional texture. *In* Ham, W.E. (Ed.), *Classification of Carbonate Rocks:* AAPG Mem., 108–121.

Ellis, D.V., 1987. *Well Logging for Earth Scientists:* New York (Elsevier).

Fisher, R.V., and Schmincke, H.-U., 1984. *Pyroclastic Rocks:* New York (Springer-Verlag).

Goldberg, D., 1997. The role of downhole measurements in marine geology and geophysics. *Rev. Geophys.,* 35:315–342.

Gradstein, F.M., Agterberg, F.P., Ogg, J.G., Hardenbol, J., van Veen, P., Thierry, J., and Huang, Z., 1995. A Triassic, Jurassic and Cretaceous time scale. *In* Berggren, W.A., Kent, D.V., Aubry, M.P., and Hardenbol, J. (Eds.), *Geochronology, Time Scales and Global Stratigraphic Correlation.* Spec. Publ.—Soc. Econ. Paleontol. Mineral. (Soc. Sediment. Geol.), 54:95–212.

Hardenbol, J., Thierry, J., Farley, M.B., Jacquin, Th., de Graciansky, P.-C., and Vail, P.R. (with numerous contributors), 1998. Mesozoic and Cenozoic sequence chronostratigraphic framework of European basins. *In* Graciansky, P.-C., Hardenbol, J., Jacquin, T., and Vail, P.R. (Eds.), *Mesozoic-Cenozoic Sequence Stratigraphy of European Basins,* Spec. Publ.—Soc. Econ. Paleontol. Mineral, 60:3–13, 763–781, and chart supplements.

Hearst, J.R., and Nelson, P.H., 1984. *Well Logging for Physical Properties:* New York (McGraw-Hill).

Hoppie, B.W., Blum, P., and the Shipboard Scientific Party, 1994. Natural gamma-ray measurements on ODP cores: introduction to procedures with examples from Leg 150. *In* Mountain, G.S., Miller, K.G., Blum, P., et al., *Proc. ODP, Init. Repts.,* 150: College Station, TX (Ocean Drilling Program), 51–59.

International Hydrographic Organization/Intergovernmental Oceanographic Commission (IHO/IOC), 1997. *General Bathymetric Chart of the Ocean (GEBCO) Digital Atlas:* London (British Oceanographic Data Centre).

Jeremiah, J., 1996. A proposed Albian to lower Cenomanian nannofossil biozonation for England and the North Sea Basin. *J. Micropaleont.,* 15:97–129.

Kennett, J.P., and Srinivasan, M.S., 1983. *Neogene Planktonic Foraminifera: A Phylogenetic Atlas:* Stroudsburg, PA (Hutchinson Ross).

Kirschvink, J.L., 1980. The least-squares line and plane and the analysis of palaeomagnetic data. *Geophys. J. R. Astron. Soc.,* 62:699–718.

Kono, M., 1980. Statistics of paleomagnetic inclination data. *J. Geophys. Res.,* 85:3878–3882.

MacKenzie, W.S., Donaldson, C.H., and Guilford, C., 1982. *Atlas of Igneous Rocks and their Textures:* Harlow, England (Longman).

Mann, P., Coffin, M., Shipley, T., Cowley, S., Phinney, E., Teagan, A., Suyehiro, K., Takahashi, N., Araki, E., Shinohara, M., and Miura, S., 1996. Researchers investigate fate of oceanic plateaus at subduction zones. *Eos,* 77:282–283.

Martini, E., 1971. Standard Tertiary and Quaternary calcareous nannoplankton zonation. *In* Farinacci, A. (Ed.), *Proc. 2nd Int. Conf. Planktonic Microfossils Roma:* Rome (Ed. Tecnosci), 2:739–785.

Mayer, L.A., Shipley, T.H., Winterer, E.L., Mosher, D., and Hagen, R.A., 1991. SeaBeam and seismic reflection surveys on the Ontong Java Plateau. *In* Kroenke, L.W., Berger, W.H., Janecek, T.R., et al., *Proc. ODP, Init. Repts.,* 130: College Station, TX (Ocean Drilling Program), 45–75.

Mazzullo, J.M., Meyer, A., and Kidd, R.B., 1988. New sediment classification scheme for the Ocean Drilling Program. *In* Mazzullo, J., and Graham, A.G. (Eds.), *Handbook for Shipboard Sedimentologists.* ODP Tech. Note, 8:45–67.

McKee, E.D., and Weir, G.W., 1953. Terminology for stratification and cross-stratification in sedimentary rocks. *Geol. Soc. Am. Bull.,* 64:381–390.

Mochizuki, K., Coffin, M., and Eldholm, O., 1998. Upper crustal structure along an E-W transect from the Nauru Basin to the north-central Ontong Java Plateau. *Eos,* 79:F869.

Mosher, D.C., Mayer, L.A., Shipley, T.H., Winterer, E.L., Hagen, R.A., Marsters, J.C., Bassinot, F., Wilkens, R.H., and Lyle, M., 1993. Seismic stratigraphy of the Ontong Java Plateau. *In* Berger, W.H., Kroenke, L.W., Mayer, L.A., et al., *Proc. ODP, Sci. Results,* 130: College Station, TX (Ocean Drilling Program), 33–49.

Munsell Color Company, Inc., 1975. *Munsell Soil Color Charts:* Baltimore, MD (Munsell).

Murray, R.W., Miller, D.J., and Kryc, K.A., 2000. Analysis of major and trace elements in rocks, sediments, and interstitial waters by inductively coupled plasma—atomic emission spectrometry (ICP-AES). *ODP Tech. Note,* 29 [Online]. Available from World Wide Web: <http://www-odp.tamu.edu/publications/tnotes/tn29/INDEX.HTM>. [Cited 2000-09-06]

Nyong, N., and Olsson, R.K., 1984. A paleoslope model of Campanian to lower Maestrichtian foraminifers in the North American Basin and adjacent continental margin. *Mar. Micropaleontol.,* 8:437–477.

Olsson, R.K., Hemleben, C., Berggren, W.A., and Huber, B.T. (Eds.), 1999. *Atlas of Paleocene Planktonic Forminifera:* Smithsonian Contrib. Paleobiol., 85.

Perch-Nielsen, K., 1985. Mesozoic calcareous nannofossils. *In* Bolli, H.M., Saunders, J.B., and Perch-Nielsen, K. (Eds.), *Plankton Stratigraphy:* Cambridge (Cambridge Univ. Press), 329–426.

Phinney, E.J., Mann, P., Coffin, M.F., and Shipley, T.H., 1999. Sequence stratigraphy, structure, and tectonic history of the southwestern Ontong Java Plateau adjacent to the North Solomon Trench and Solomon Islands arc. *J. Geophys. Res.,* 104:20,449–20,466.

Rider, M., 1996. *The Geological Interpretation of Well Logs* (2nd ed.): Caithness (Whittles Publishing).

Roth, P.H., 1978. Cretaceous nannoplankton biostratigraphy and oceanography of the northwestern Atlantic Ocean. *In* Benson, W.E., Sheridan, R.E., et al., *Init. Repts. DSDP,* 44: Washington (U.S. Govt. Printing Office), 731–759.

Sass, J.H., Kennelly, J.P., Jr., Smith, E.P., and Wendt, W.E., 1984. Laboratory line-source methods for the measurement of thermal conductivity of rocks near room temperature. *Open-File Rep.—U.S. Geol. Surv.,* 84–91.

Schlumberger, 1989. *Log Interpretation Principles/Applications:* Houston (Schlumberger Educ. Services), SMP–7017.Schlumberger, 1989.

————, 1994. *IPL Integrated Porosity Lithology:* Houston (Schlumberger Wireline and Testing), SMP-9270.

Serra, O., 1984. *Fundamentals of Well-Log Interpretation* (Vol. 1): *The Acquisition of Logging Data:* Dev. Pet. Sci., 15A.

————, 1986. *Fundamentals of Well-Log Interpretation* (Vol. 2): *The Interpretation of Logging Data*. Dev. Pet. Sci., 15B.

————, 1989. *Formation MicroScanner Image Interpretation:* Houston (Schlumberger Educ. Services), SMP-7028.

Shipboard Scientific Party, 1991. Explanatory notes. *In* Davies, P.J., McKenzie, J.A., Palmer-Julson, A., et al., *Proc. ODP, Init. Repts.,* 133 (Pt. 1): College Station, TX (Ocean Drilling Program), 31–58.

————, 1997. Explanatory notes. *In* Eberli, G.P., Swart, P.K., Malone, M.J., et al., *Proc. ODP, Init. Repts.,* 166: College Station, TX (Ocean Drilling Program), 43–65.

————, 2001. Explanatory notes. *In* Christie, D.M., Pedersen, R.B., Miller, D.J., et al., *Proc. ODP, Init. Repts.,* 187, 1–42 [Online]. Available from World Wide Web: <http://www-odp.tamu.edu/publications/187_IR/VOLUME/CHAPTERS/IR187_02.PDF>. [Cited 2000-09-06]

Sikora, P.J., Bergen, J.A., and Farmer, C.L., 1999. Chalk palaeoenvironments and depositional model, Valhall–Hod fields, southern Norwegian North Sea. *In* Jones, R.W., and Simmons, M.D. (Eds.), *Biostratigraphy in Production and Development Geology,* Spec. Publ.—Geol. Soc. London, 152:113–137.

Sikora, P.J., and Olsson, R.K., 1991. A paleoslope model of late Albian to early Turonian foraminifers of the west Atlantic Margin and Northern Atlantic Basin. *Mar. Micropaleontol.,* 8:25–72.

Sissingh, W., 1977. Biostratigraphy of Cretaceous calcareous nannoplankton. *Geol. Mijnbouw,* 56:37–65.

————, 1978. Microfossil biostratigraphy and stage-stratotypes of the Cretaceous. *Geol. Mijnbouw,* 57:433–440.

Sliter, W.V., 1989. Biostratigraphic zonation for Cretaceous planktonic foraminifers examined in thin section. *J. Foraminiferal Res.,* 19:1–19.

Toumarkine, M., and Luterbacher, H., 1985. Paleocene and Eocene planktic foraminifera. *In* Bolli, H.M., Saunders, J.B., and Perch-Nielsen, K. (Eds.), *Plankton Stratigraphy:* Cambridge (Cambridge Univ. Press), 87–154.

Urmos, J., Wilkens, R.H., Bassinot, F., Lyle, M., Marsters, J.C., Mayer, L.A., and Mosher, D.C., 1993. Laboratory and well-log velocity and density measurements from the Ontong Java Plateau: new in-situ corrections to laboratory data for pelagic carbonates. *In* Berger, W.H., Kroenke, L.W., Mayer, L.A., et al., *Proc. ODP, Sci. Results,* 130: College Station, TX (Ocean Drilling Program), 607–622.

Vacquier, V., 1985. The measurement of thermal conductivity of solids with a transient linear heat source on the plane surface of a poorly conducting body. *Earth Planet. Sci. Lett.,* 74:275–279.

Van Morkhoven, F.P.C.M., Berggren, W. A., Edwards, A.S., 1986. Cenozoic cosmopolitan deep-water benthic foraminifers. *Bull. Cent. Rech. Explor.-Prod. Elf-Aquitaine* 11:Pau (Elf Aquitaine).

Von Herzen, R.P., and Maxwell, A.E., 1959. The measurement of thermal conductivity of deep-sea sediments by a needle-probe method. *J. Geophys. Res.,* 64:1557–1563.

Wentworth, C.K., 1922. A scale of grade and class terms of clastic sediments. *J. Geol.,* 30:377–392.

Zidjerveld, J.D.A., 1967. A.C. demagnetization of rocks: analysis of results. *In* Collinson, D.W., Creer, K.N., and Runcorn, S.K. (Eds.), *Methods in Paleomagnetism:* Amsterdam (Elsevier), 254–286.

Figure F1. Schematic examples of numbered core sections from Hole 1183A.

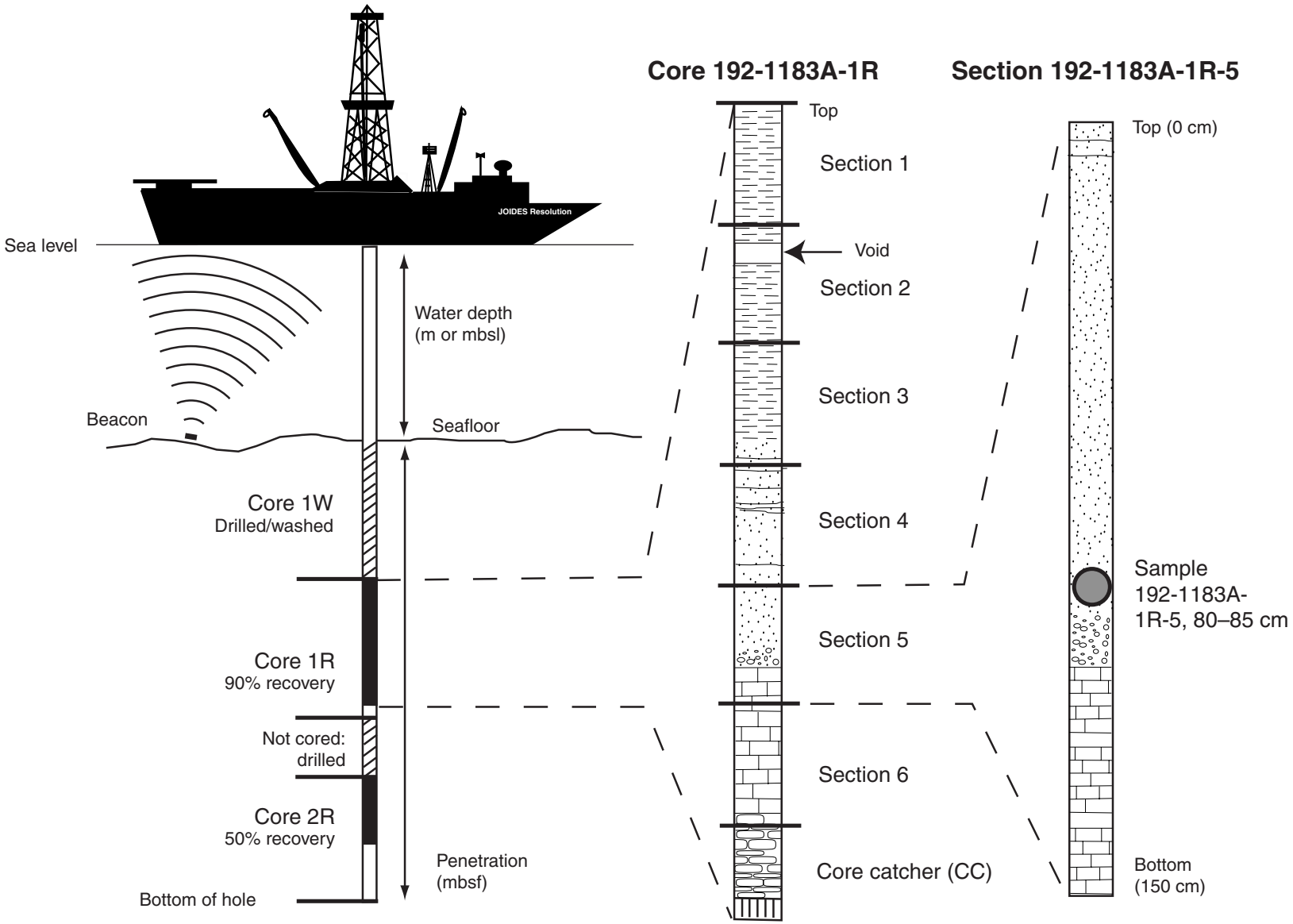

Figure F2. Bathymetry of the Ontong Java Plateau (IHO/IOC, 1997). Solid circles = previous ODP drill sites that recovered igneous basement; open circles = sites that bottomed in sediment; solid stars = proposed primary drill sites (OJ) for Leg 192; open stars = proposed alternate drill sites. Drilled sites also include ODP site numbers shown in parentheses. Seismic lines used to select the sites = black lines with cruise identifiers (KH = *Hakuho Maru,* EW = *Maurice Ewing,* TW = *Thomas Washington, Charcot*) and numbers in small font size. SB = sonobuoy. Triangles = ocean-bottom seismometer and sonobuoy deployments. The contour interval is 1000 m.

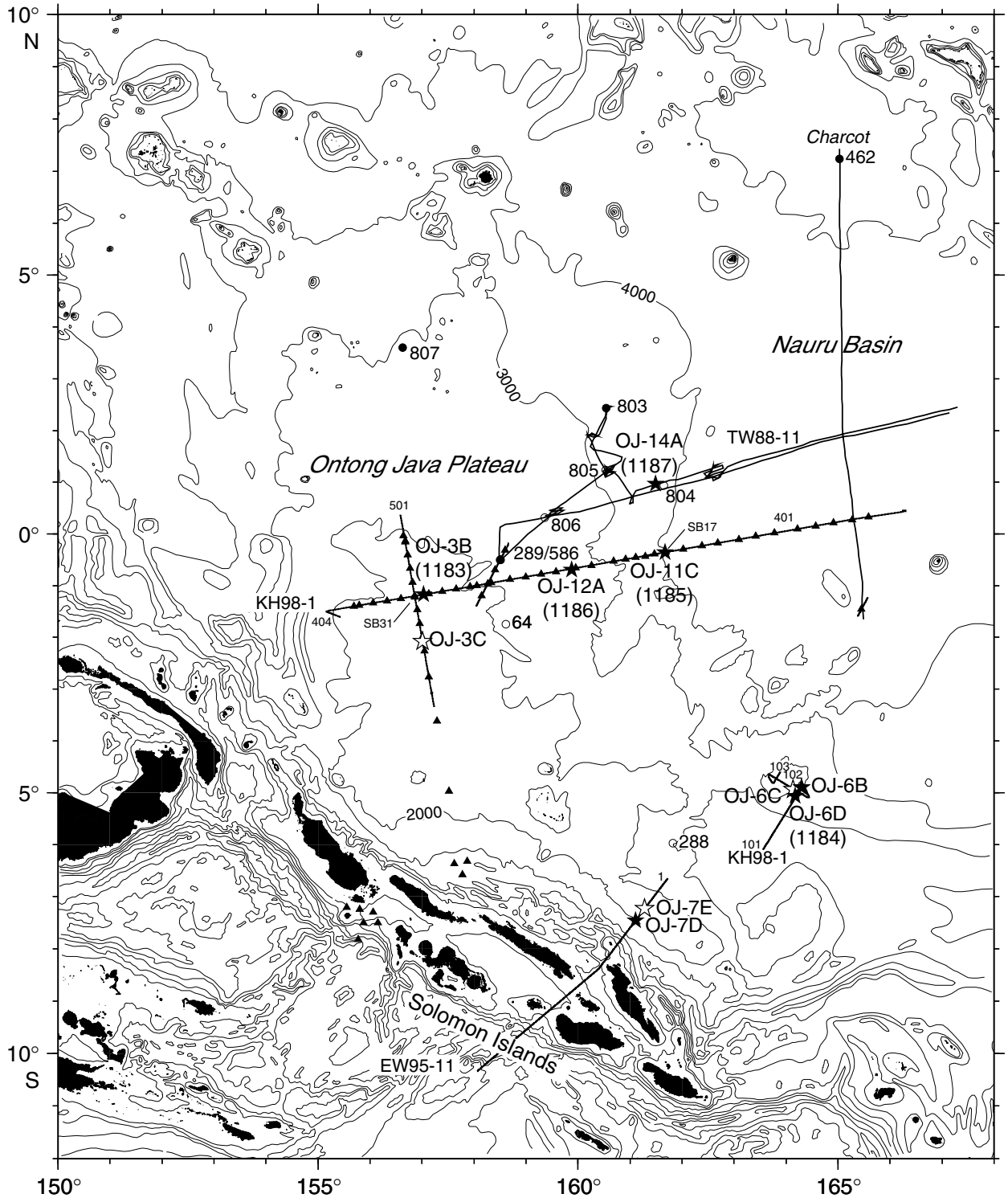

Figure F3. Example of a core-description summary (barrel sheet) generated by AppleCORE. For Leg 192 barrel sheets, see the "Core Descriptions" contents list.

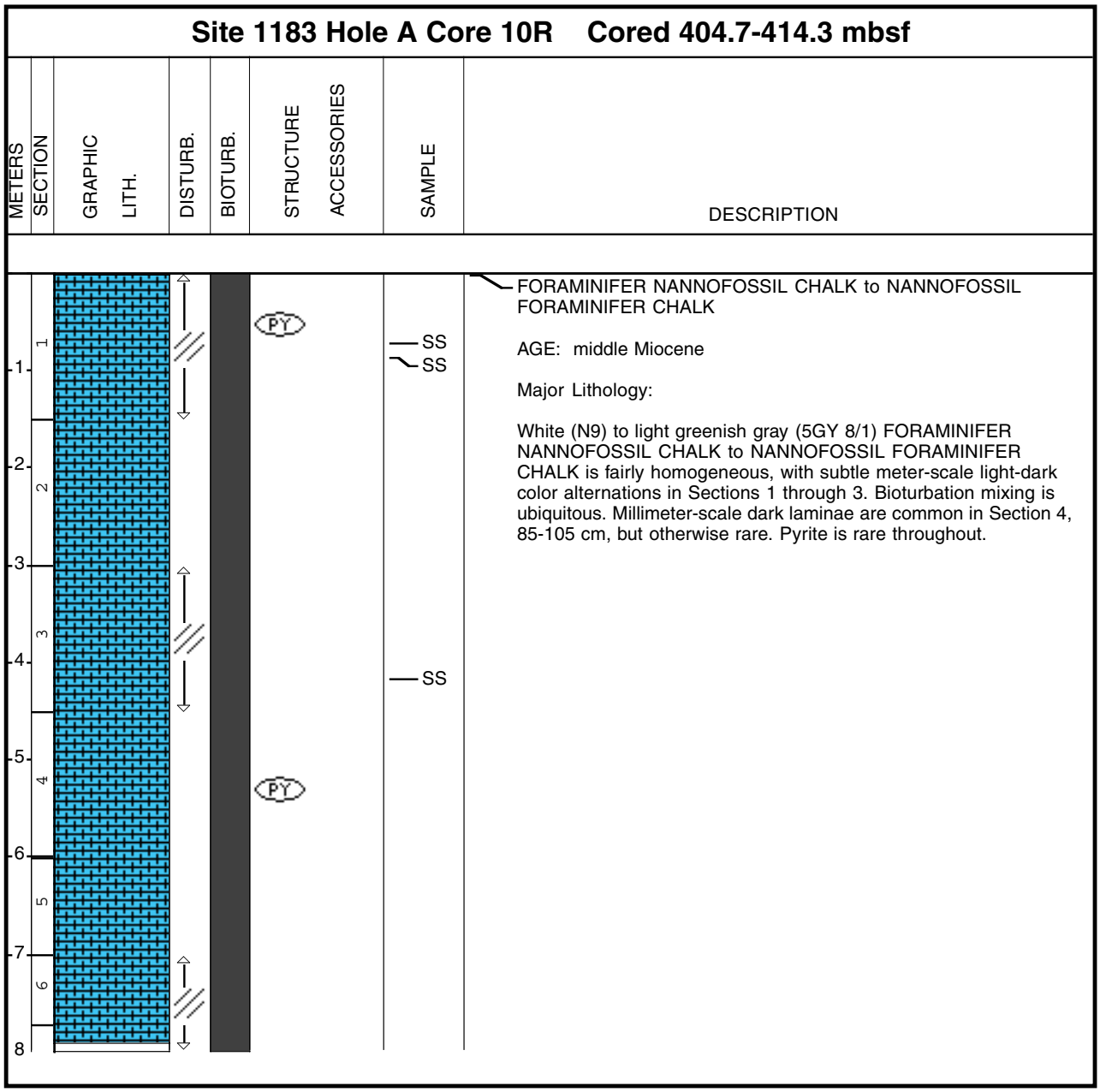

Figure F4. Key to symbols used on barrel sheets during Leg 192.

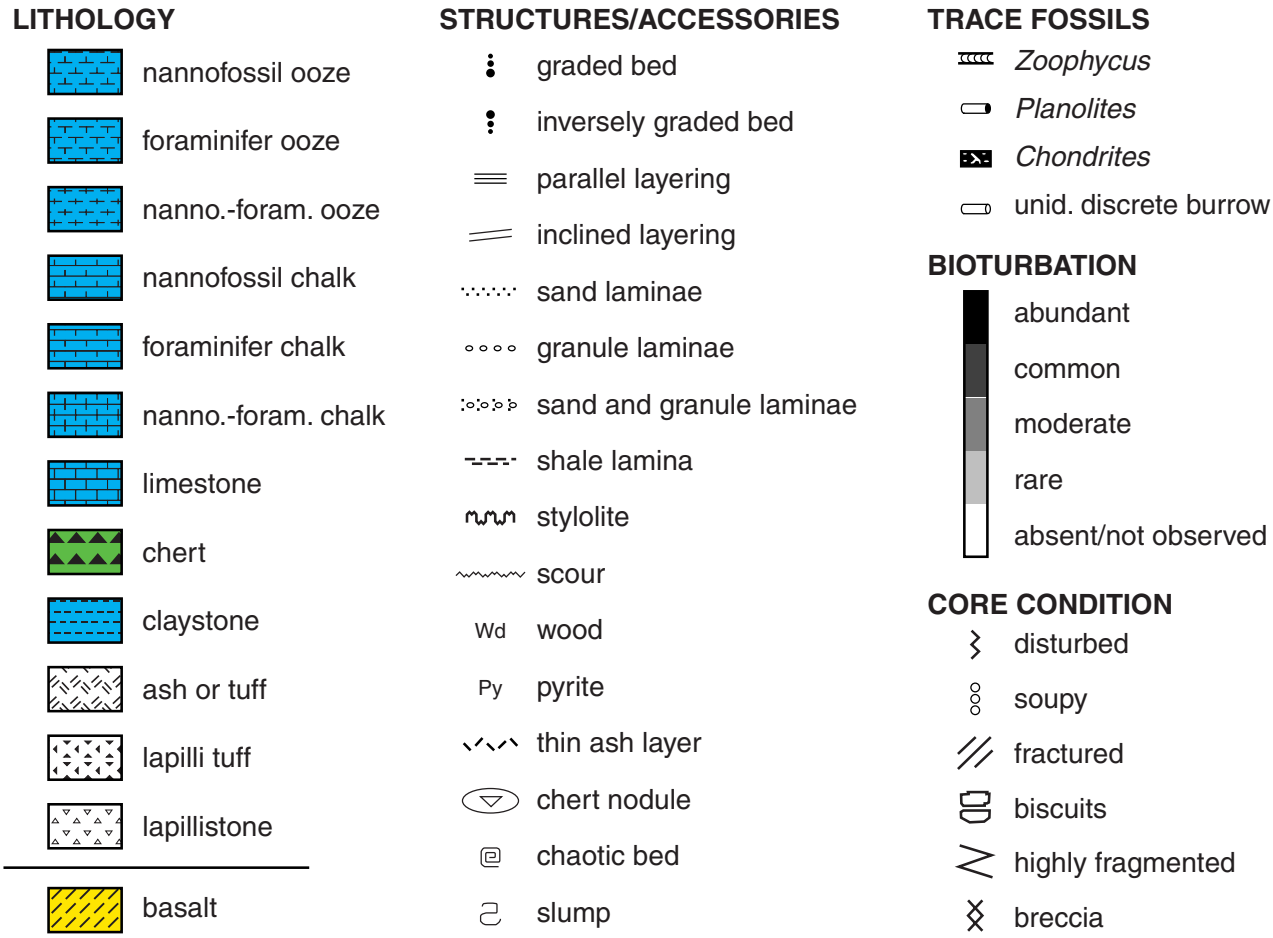

SAMPLE CODES

SS smear slide	XRD X-ray diffraction	PAL shipboard micropaleontology
CAR carbonate	THS thin section	

Figure F5. Classification scheme for granular sediment used during Leg 192 (modified from Mazzullo et al., 1988).

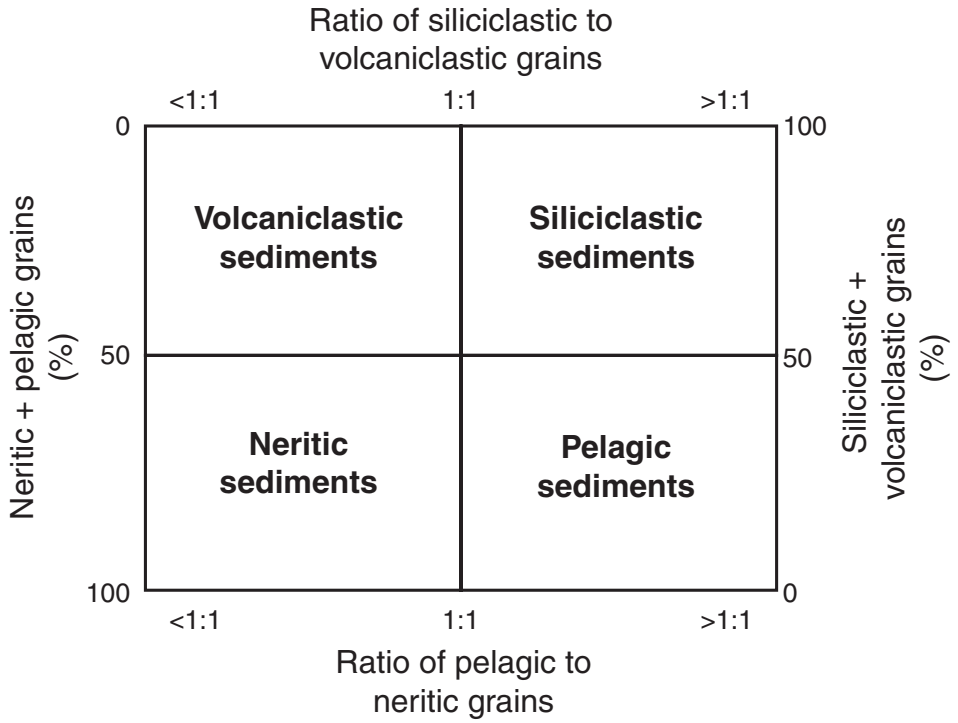

Figure F6. Coordinate systems of Ocean Drilling Program (ODP) cores and discrete samples. **A.** Orientation of the discrete samples (12-cm³ cylindrical minicores and 7-cm³ plastic cubes) obtained from the working halves. **B.** The coordinate systems of both the archive and working halves of cores for paleomagnetic measurements.

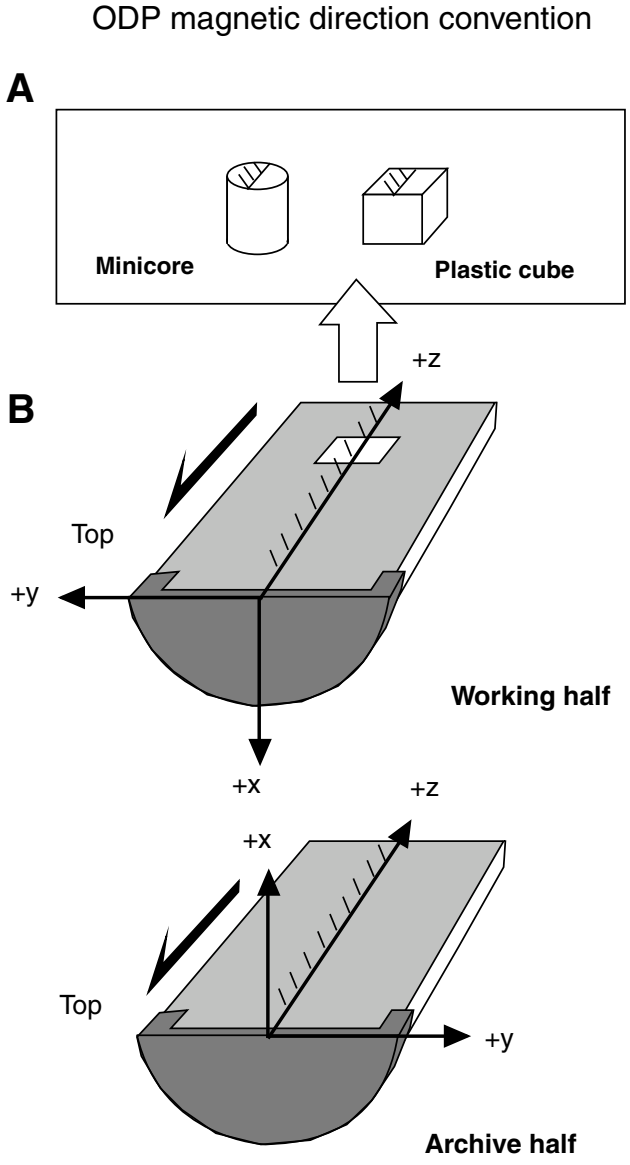

Figure F7. The geophysical and Formation MicroScanner/sonic tool strings used during Leg 192. HNGS = hostile-environment natural gamma ray sonde, APS = accelerator porosity sonde, HLDS = hostile-environment lithodensity sonde, DITE-SFR = phasor dual induction–spherically focused resistivity tool, TAP = high-resolution temperature/acceleration/pressure tool, DSI = dipole shear sonic imager, NGT = natural gamma spectrometry tool, GPIT = general-purpose inclinometer tool, FMS = Formation MicroScanner logging tool.

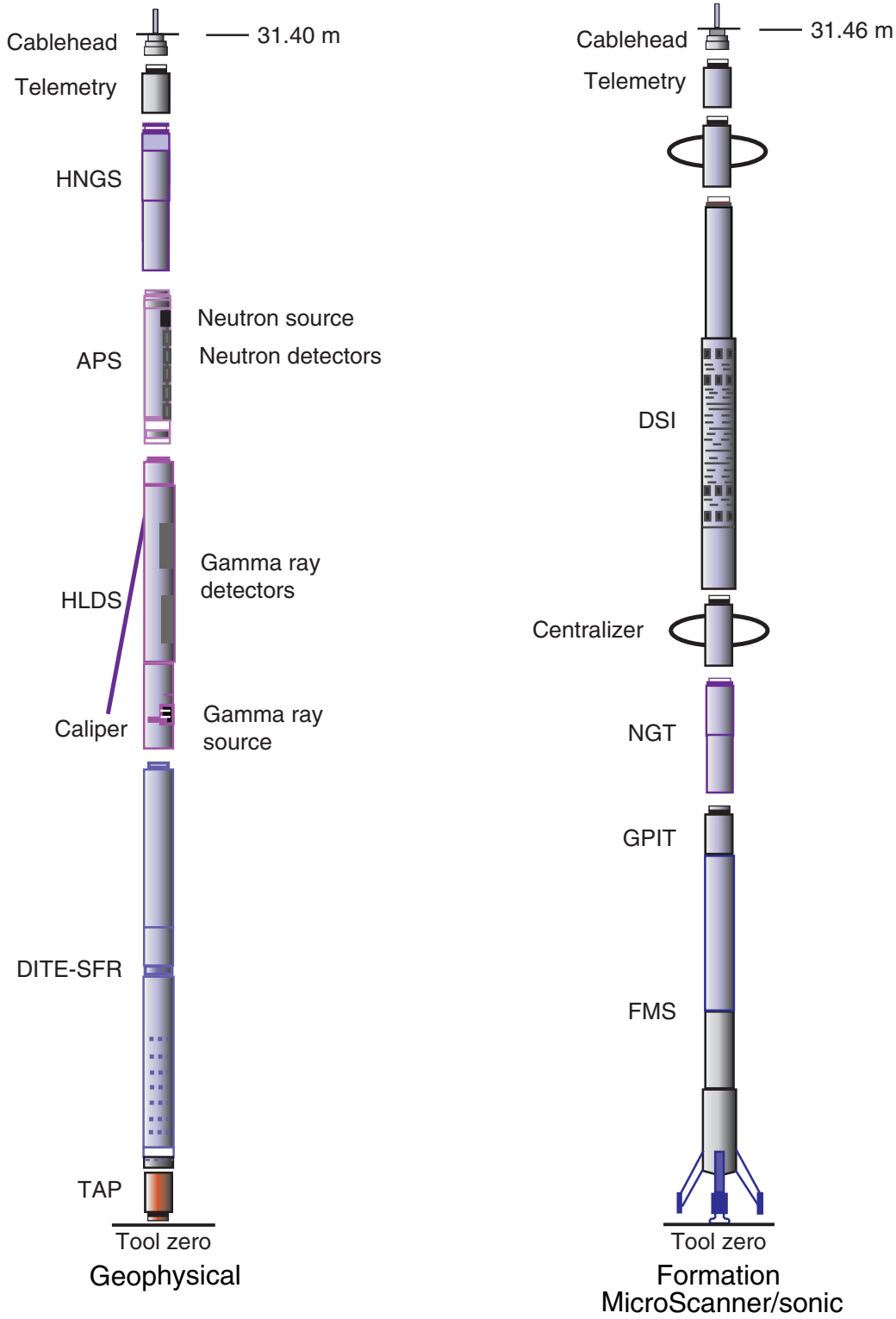

Figure F8. Schematic diagram of the Formation MicroScanner pad.

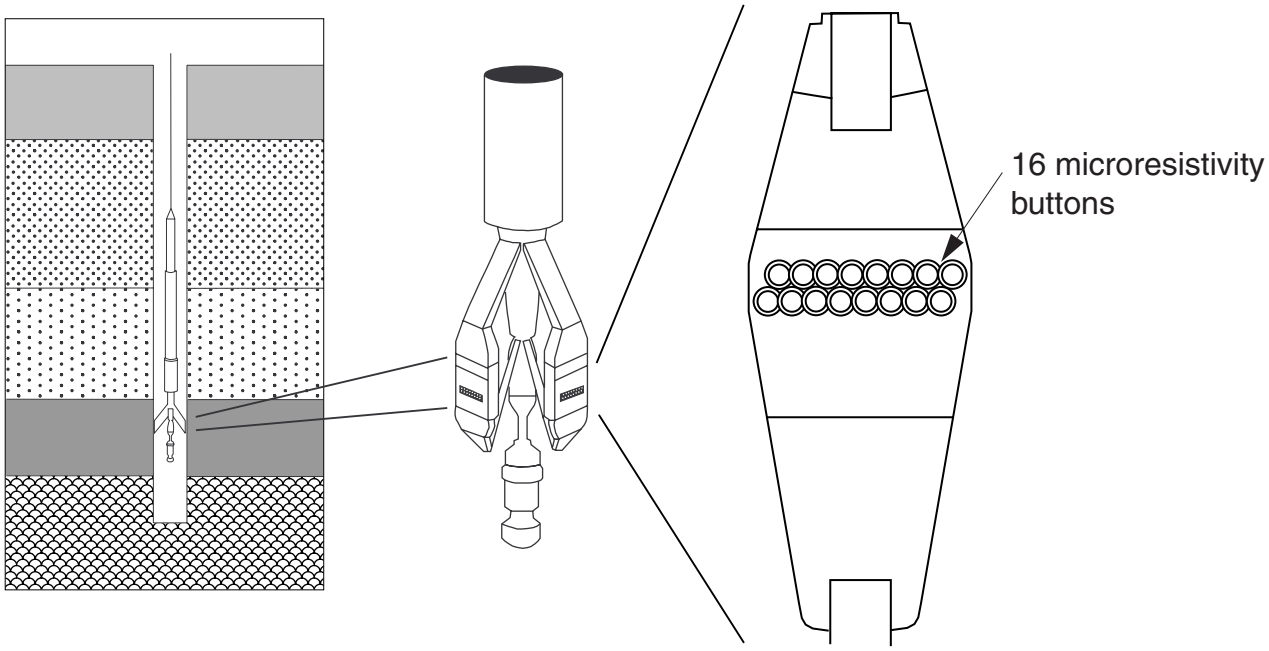

Table T1. Acquisition parameters of seismic reflection data used in selecting proposed drill sites on the Ontong Java Plateau.

	Hakuho Maru KH98-1 Leg 2	*Maurice Ewing* 95-11	*Thomas Washington* 88-11
Year	1998	1995	1988
Designation	KH98-1	EW95-11	TW88-11
Navigation	GPS	GPS	GPS/Transit
Source	1–4 air guns	20 air guns	1 water gun
Volume	4.5 L/1000-3400 in^3	8510 L/in^3	80 L/in^3
Shot interval (m)	~50	~50	~40
Sample interval (ms)	2	2	1
Record length (s)	8 and 16	16	3-9
Streamer length (m)	300 and 1200	3000	100
Number of groups	24 and 48	120	1
Group interval (m)	12.5 and 25	25	NA
Processing	Migration	Migration	NA

Notes: GPS = Global Positioning System. Two values in columns indicate single-channel seismic/multichannel seismic. NA = not applicable.

Table T2. ICP-AES run parameters.

Standard	Wavelength (nm)	Slit width (nm)*	Integration time per calculation point (s)	Voltage (V)	Mode	Increment between points (nm)†	Number of calculation points
Al	396.150	20/16	0.5	731	2	0.0270	5
Ca	393.370	20/16	0.5	351	2	0.0180	5
Fe	259.940	20/16	4.0	732	5	0.0020	1
K	766.490	20/16 Alk	0.5	993	2	0.0022	5
Mg	285.213	20/16	4.0	553	5	0.0022	1
Mn	257.610	20/16	4.0	643	5	0.0020	1
Na	589.592	20/16 Alk	0.5	632	2	0.0021	5
P	178.229	20/16	0.5	933	2	0.0018	5
Si	251.611	20/51	0.5	612	2	0.0028	5
Si	212.412	20/51	0.5	652	2	0.0030	5
Si	288.158	20/51	0.5	623	2	0.0029	5
Ti	334.941	20/16	0.5	651	2	0.0018	5
Ba	455.400	20/16	4.0	622	5	0.0250	1
Cr	267.716	20/16	4.0	993	5	0.0190	1
Ni	231.604	20/16	0.5	990	2	0.0021	1
Sc	361.384	20/16	4.0	753	5	0.0018	1
Sr	407.771	20/16	0.5	572	2	0.0026	5
V	292.402	20/16	4.0	993	5	0.0021	1
Y	371.030	20/16	4.0	693	5	0.0027	1
Zr	343.823	20/16	0.5	673	2	0.0018	5

Notes: The above settings are stored in the software as "BAS192 Method Acquisition Parameter." * = widths of the entrance and exit slits. Alk = an increase in sheath gas flow from 0.15–0.2 L/min to 0.8 L/min for analysis of these elements. † = the interval between each of the calculation points in Mode 2 or the calculation window (in nanometers) that constitutes the single point in Mode 5.

Table T3. Typical values for USGS standards analyzed by ICP-AES, Leg 192.

Standard analyzed:	BHVO-2				BCR-2				BIR-1			
Site:	1183	1184 and 1185	1186 and 1187	Certified	1183	1184 and 1185	1186 and 1187	Certified	1183	1184 and 1185	1186 and 1187	Certified
Major element (wt%):												
SiO_2	49.56	49.56	49.82	49.85	54.47	53.73	53.96	54.10	47.45	48.26	48.11	47.770
TiO_2	2.77	2.77	2.75	2.73	2.32	2.24	2.24	2.26	0.96	0.95	0.96	0.960
Al_2O_3	13.87	13.87	13.88	13.53	13.72	13.65	13.55	13.50	15.80	15.78	15.88	15.350
Fe_2O_3*	12.01	12.01	12.86	12.34	13.97	13.37	13.55	13.80	11.77	11.19	10.98	11.260
MnO	0.17	0.17	0.18	0.20	0.20	0.22	0.21	0.24	0.17	0.19	0.18	0.171
MgO	7.29	7.29	7.40	7.23	3.70	3.79	3.60	3.59	9.75	9.81	9.60	9.680
CaO	11.34	11.34	11.29	11.43	7.25	7.21	7.08	7.12	13.04	13.13	13.18	13.240
Na_2O	2.27	2.27	2.24	2.22	3.26	3.15	3.21	3.16	1.86	1.81	1.85	1.750
K_2O	0.57	0.57	0.70	0.52	1.96	2.00	1.79	1.79	BD	0.02	0.03	0.027
P_2O_5	0.27	0.27	0.27	0.27	0.33	0.32	0.35	0.35	0.11	0.03	0.01	0.046
Total:	99.83	99.83	101.40		100.86	99.89	99.54		100.77	101.31	100.79	
Trace element (ppm):												
Ni	120	120	121	119	12	8	14	20	175	175	173	166
Cr	282	282	287	280	15	20	10	18	390	380	383	382
V				317		413	410	416		317	300	310
Zr	179	179	177	172	193	196	192	188	14	15	12	16
Sc	33	33	35	32	36	35	34	33	48	45	43	44
Y	27	27	26	26	39	36	38	37	18	16	19	16
Sr	385	385	389	389	340	335	329	346	107	106	109	108
Ba	136	136	138	130	716	710	686	683	7	6	7	7

Notes: All values are averages of the BHVO-2 and K-1919 reductions of each run. Only the K-1919 reduction was used for Site 1183 samples. Certified vanadium values are unavailable for K-1919. BHVO-2, BCR-2, and BIR-1 are USGS-certified basalt standards. K-1919 is a noncertified laboratory standard from the University of Massachusetts. * = total Fe expressed as Fe_2O_3. BD = below detection limit.

Table T4. Abbreviations used in the alteration and vein/structure logs.

Common colors			Primary and secondary minerals*		Apparent vein orientation	
Color name	Abbreviation	Munsell reference	Mineral	Abbreviation	Orientation	Abbreviation
Black	Blk	10YR 2/1	Celadonite	Cel	Inclined	INC
White	Wht	2.5Y N8	Calcium carbonate	CO_3	Curved	CUR
Brown	Brn	10YR 4/3	Iron oxyhydroxides	FeOx	Horizontal	H
Yellowish brown	Yel-Brn	10YR 5/8	Olivine	Ol	Vertical	V
Dark brown	Dk Brn	10YR 3/3	Plagioclase	Pl	Subhorizontal	SH
Olive	Olv	5Y 4/3	Pyrite	Py	Subvertical	SV
Green	Grn	10GY 4/4	Saponite	Sap		
Yellowish green	Yel-Grn	10Y 7/6	Smectite	Sm		
Dark green	Dk Grn	10GY 3/2	Zeolite	Zeol	Other	
Dusky green	Grn-Gr	5G 3/2	Manganese oxyhydroxides	MnOx	<<	Much less than
Grayish green	Gr-Grn	5G 5/2	Chalcedony	Chal	HF	Hairline fracture
Gray	Gr	10Y 5/1	Quartz	Qtz	->	Altered to
Dark gray	Dk Gr	10YR 4/1	Pyroxene	Pyx	tr	Trace (<1%)
Dark yellowish brown	DYB	10YR 4/6			Sed.	Sediment
Light yellowish brown	LYB	10YR 6/4			App.	Apparent
Pink	Pink	10R 8/4			Ident.	Identifier

Note: * = other mineral names and colors are spelled out.

Table T5. Alteration log form.

Leg 192 Alteration Log																																			
Identifiers									Rock Color/Alteration Type																Phenocrysts						Groundmass		Vesicles & Miarolitic Cavities		Comments
Unit	Core	Sec	Piece #	Interval top	Interval bot	length (cm)	Depth core top	Depth Piece Top	% Blk	% Wht	% Brn	% Yel-Brn	% Dk Brn	% Olv	% Grn	% Yel-Grn	% Dk Grn	% Grn-Gr	% Gr-Grn	% Gr	% Dk Gr	% DYB	% LYB	% Pink	Ol % alt	2nd min	Pl % alt	2nd min	Pyx % alt	2nd min	% alt	% altrd glass	(%)	Minerals and %	

Table T6. Vein/structure log form.

Leg 192 Vein/Structure Log																																										
Identifiers					Position		Vein				Vein Minerals									Halo										Comments	Structural Measurements											
																															Measurements				Calculated			Measured (real)				
Unit	Core	Sec	piece #	Vein Ident.	mbsf top section	mbsf m	cm top	cm bot	(mm) Width	App. Orient.	% Sm	% Cel	% CO3	% Py	% Qtz	% Sed.	% MnOx	% FeOx	% Zeol	Color	Width	Sm	CO3	FeOx	Py	Zeol	MnOx	Cel	Sed		App. Dip 1	Dir.	App. Dip 2	Dir.2 2	Strike	Dip	Dip Dir.	Strike	Dip	Dip Dir.	Vein Density veins/m	Vein Abundance mm/m

Table T7. Structural geology checklist.

Fractures:
Fracture density defined as the number of fractures per meter of core
Veins:
Vein orientation
Average vein width
Mineral infilling
Vein fabric
Crack seal events (# of events)
Vein abundance defined as the cumulative width of veins per meter of core
Wall-rock alteration (width and characteristics of halo)
Crosscutting relations of veins
Vein cluster
Cluster thickness
Number of veins in cluster
Composition of veins
Orientation
Shear zones:
Shear-zone thickness
Lineations
Deformation bands
Color
Thickness
Mineral composition
Number of bands within array
Faults:
Orientation of fault zone
Fault-zone thickness
Shear sense (offset, Reidel shears, mineral lineation)
Amount of offset
Nature of gouge
Composition of mineral infilling
Slickenlines orientation
Cataclasites:
Clast size
Clast shape
Clast composition
Matrix composition (gouge or secondary minerals)
Breccias:
Matrix or clast supported
Percent matrix
Matrix composition
Clast size
Angular vs. rounded clasts
Clast composition
Origin (hydraulic vs. fault)
Sedimentary structures:
Layering (spacing between laminae)
Clastic dikes
Igneous contacts:
Chilled margins
Dike width
Crosscutting relations:
Basalt flows or sediments
Dikes
Sills
Veins
Shear zones
Faults, cataclasites, breccias

Table T8. Logging tool and measurement acronyms.

Tool string	Tool	Output	Physical significance	Unit
Geophysical:	HNGS*		Hostile-environment natural gamma ray sonde	
		HSGR	Standard (total) gamma ray	gAPI
		HCGR	Computed gamma ray (HSGR minus uranium contribution)	gAPI
		HFK	Formation potassium	Fraction
		HTHO	Thorium	ppm
		HURA	Uranium	ppm
	APS*		Accelerator porosity sonde	
		APLC	Near array porosity (limestone corrected)	Fraction
		FPLC	Far array porosity (limestone corrected)	Fraction
		SIGF	Neutron-capture cross section of the formation (Sf)	cu
		STOF	Tool standoff (computed distance from borehole wall)	in
	HLDS*		Hostile-environment lithodensity sonde	
		RHOM	Bulk density (corrected)	g/cm^3
		PEF	Photoelectric effect	$barn/e^-$
		LCAL	Caliper-measure of borehole diameter	in
		DRH	Bulk density correction	g/cm^3
	DITE–SFR*		Phasor dual induction–spherically focused resistivity tool	
		IDPH	Deep induction phasor-processed resistivity	Ωm
		IMPH	Medium induction phasor-processed resistivity	Ωm
		SFLU	Shallow spherically focused resistivity	Ωm
	TAP		High-resolution temperature/acceleration/pressure tool	°C, m/s^2, psi
FMS/Sonic:	NGT*		Natural-gamma spectrometry tool	
		SGR	Standard (total) gamma ray	gAPI
		CGR	Computed gamma ray (SGR minus uranium contribution)	gAPI
		POTA	Potassium	wet wt%
		THOR	Thorium	ppm
		URAN	Uranium	ppm
	DSI*		Dipole shear sonic imager	
		DTCO	Compressional wave transit time	µs/ft
		DTSM	Shear wave transit time	µs/ft
		DTST	Stoneley wave transit time	µs/ft
	GPIT*		General purpose inclinometer tool	
		FX, FY, FZ	Magnetic field (three orthogonal directions)	Oersted
		AX, AY, AZ	Acceleration (three orthogonal directions)	m/s^2
	FMS*		Formation MicroScanner	
			Oriented images of borehole wall microresistivity	Ωm

Note: * = Schlumberger trademark tools.

Table T9. Specifications of logging tools used during Leg 192.

Tool string	Approximate logging speed (m/hr)	Individual tools	Properties measured	Tool length (m)	Sampling interval (cm)	Approximate vertical resolution (cm)	Approximate depth of investigation (cm)
Run 1: Geophysical	274	HNGS*	Natural gamma ray	2.59	15	45	Variable
		APS*	Porosity	3.96	5 and 15	30	15
		HLDS*	Bulk density, PEF	7.03	15	38	15
		DITE-SFR*	Resistivity	9.53	15	200/150/76	150/76/38
		TAP	Temperature	2.71	1/s	NA	NA
			Tool acceleration		4/s		
			Pressure		1/s		
Run 2: FMS*/Sonic	274	FMS*	Resistivity image	7.72	0.25	0.5	15
		NGT*	Natural gamma ray	2.61	15	45	Variable
		GPIT*	Tool orientation, magnetic field	(In FMS)	1 or 15	NA	NA
		DSI*	Sonic velocity	15.50	15	110	15-30

Notes: * = Schlumberger trademark tools. See Table **T8,** p. 52, for definitions of acronyms. NA = not applicable